Skin mesenchymal niches maintain and protect AML-initiating stem cells

Running title: Extramedullary mesenchymal cell niche in AML

Lakshmi Sandhow[1], Huan Cai[1]#, Elory Leonard[1]#, Pingnan Xiao[1], Luana Tomaipitinca[1], Alma Månsson[1], Makoto Kondo[1&], Xiaoyan Sun[2], Anne-Sofie Johansson[1], Karl Tryggvason[3], Maria Kasper[2], Marcus Järås[4], Hong Qian[1*]

[1]Center for Hematology and Regenerative Medicine, Department of Medicine Huddinge, Karolinska Institute, Karolinska University Hospital, SE-141 86 Stockholm, Sweden;

[2]Department of Cell and Molecular Biology, Karolinska Institute, 171 77, Stockholm, Sweden;

[3]Department of Medical Biochemistry and Biophysics, Karolinska Institute, Stockholm, 17177, Sweden;

[4]Department of Clinical Genetics, Lund University, Lund 22184, Sweden.

[&]Current address: Cell Sheet Tissue Engineering Center (CSTEC), Department of Pharmaceutics and Pharmaceutical Chemistry, Health Sciences, University of Utah, 30 South 2000 East, Salt Lake City, Utah 84112, USA.

# equal contribution

***Corresponding author:** Hong Qian, hong.qian@ki.se

Word count:5066 word, 27538 characters excluding figure legends and references

Abstract word count: 149

Figures: 8 main figures, 5 supplemental figures

Non-standard abbreviations: AML, acute myeloid leukemia; MSCs, mesenchymal stem cells; MPCs, mesenchymal progenitor cells; LSCs, leukemia-initiating stem cells; HSCs, hematopoietic stem cells; HSPCs, hematopoietic stem and progenitor cells; Ebf2, Early B-cell factor 2; BM, bone marrow; Ara-C, cytarabine; NS, normal saline; FACS, fluorescence-activated cell sorting; CFU-C, colony forming unit in culture; CAFC, cobblestone area-forming cells; DPC, dermal panniculus carnosus; CFU-F, colony-forming unit in fibroblast; PαS, PDGFRa/CD140a and SCA1-expressing stromal cells.

A 40-word summary: Sandhow et al have in transplantation-induced AML mouse models demonstrated the leukemia-regenerating capacity of AML cells infiltrated in the skin and the role of skin mesenchymal niches in maintaining/protecting AML cells, providing new insight into the pathology of leukemia cutis.

Abstract (149)

Leukemia cutis or leukemic cell infiltration in skin is one of the common extramedullary manifestations of acute myeloid leukemia (AML) and signifies a poorer prognosis. However, its pathogenesis and maintenance remain understudied. Here, we report massive AML cell infiltration in the skin in a transplantation-induced MLL-AF9 AML mouse model. These AML cells could regenerate AML post-transplantation. Prospective niche characterization revealed that skin harbored mesenchymal progenitor cells (MPCs) with a similar phenotype as BM mesenchymal stem cells. These skin MPCs protected AML-initiating stem cells (LSCs) from chemotherapy *in vitro* partially via mitochondrial transfer. Furthermore, *Lama4* deletion in skin MPCs promoted AML LSC proliferation and chemoresistance. Importantly, more chemoresistant AML LSCs appeared to be retained in *Lama4*$^{-/-}$ mouse skin post-cytarabine treatment. Our study reveals the characteristics and previously unrecognized roles of skin mesenchymal niches in maintaining and protecting AML LSCs during chemotherapy, meriting future exploration of their impact on AML relapse.

Key words: Early B-cell Factor 2, skin, mesenchymal progenitor cells, acute myeloid leukemia, stem cell niche, leukemic stem cells, drug resistance, cytarabine, bone marrow, mice

Introduction

Leukemia cutis (leukemic cell infiltration in skin) is one of the commonly observed extramedullary manifestations in acute myeloid leukemia (AML) (Bakst et al., 2011; Gouache et al., 2018) It is associated with poor survival (Gouache et al., 2018; Krooks and Weatherall, 2018; Wang et al., 2019). However, our understanding of its pathogenesis is very limited. This has been mainly due to lack of knowledge about the extramedullary niches where AML cells infiltrate and are maintained.

For decades, great efforts have been put to elucidate the contribution of the hematopoietic niche in bone marrow (BM) to normal and malignant hematopoiesis. The BM niche consists of various types of cells including mesenchymal stem cells (MSCs), mesenchymal progenitor

63 cells (MPCs), osteoblasts and endothelial cells. Accumulating evidence has shown that BM
64 MSCs and MPCs play important roles in maintaining normal hematopoiesis and in the
65 development of myeloid malignancies including AML (Hoggatt et al., 2016; Xiao et al., 2018b).
66 Molecular alterations in these niches could lead to malignant transformation of hematopoietic
67 cells (Dong et al., 2016; Raaijmakers et al., 2010; Xiao et al., 2018a). During leukemia
68 development, the leukemic cells can alter the BM niche, which renders the niche to become
69 favorable for leukemic cell growth but harmful for normal hematopoiesis (Hanoun et al., 2014;
70 Jeong et al., 2018; Kim et al., 2015; Schepers et al., 2013; Xiao et al., 2018b). Using a *Cre-*
71 *LoxP* mouse model allowing for selective deletion of the MSC population, we have shown that
72 loss of MSCs accelerates AML progression (Hanoun et al., 2014; Xiao et al., 2018b). However,
73 these markers are not unique for the mesenchymal cells in BM, thus, it is not clear whether the
74 mesenchymal cell niches in extramedullary organs like skin are also affected, thereby
75 contributing to the AML progression.

76 Besides BM, extramedullary organs such as adipose tissue have been reported to
77 accommodate hematopoietic stem and progenitor cells (HSPCs) in the stromal vascular
78 fraction (Han et al., 2010). In blast crisis of chronic myeloid leukemia, the gonadal white
79 adipose tissue is infiltrated by leukemic cells that adapt to the extramedullary niche and
80 transform into resistant leukemia-initiating stem cells (LSCs) marked by CD36 expression (Ye
81 et al., 2016).These findings indicate that extramedullary organs may serve as niches for HSPCs
82 and LSCs.

83 Existing evidence suggests that skin might contain an MSC-like cell population (Kimlin and
84 Virador, 2013; Toma et al., 2001; Vaculik et al., 2012; Viswanathan et al., 2019). However,
85 their biological properties and contribution to hematopoiesis and leukemia remain unexplored.
86 Knowledge of this would be essential for understanding the pathology of extramedullary
87 leukemia in the skin, and would thus provide new insights into identifying new potential
88 therapeutic targets that may be translated into new treatment strategies for AML patients with
89 leukemia cutis.

90 We here in a transplantation-induced AML mouse model detected massive infiltration of
91 AML cells in the skin. Importantly, these skin AML cells at steady-state or post-chemotherapy
92 could regenerate AML post-secondary transplantation even with a low dose of 10 cells/mouse.
93 Characterization of the AML niche revealed the molecular features and developmental
94 hierarchy of the skin MPCs. The MPCs expressing Early B-cell Factor 2 (Ebf2) contribute to
95 mesenchymal cell turnover in the skin and were reduced post-AML onset. The skin MPCs
96 could maintain and protect AML LSCs, and loss of *Lama4* in skin MPCs promoted AML cell

97 maintenance and resistance to chemotherapy. Altogether, our study revealed the characteristics
98 and a previously unrecognized role of skin MPCs in maintaining AML LSCs during AML
99 development and chemotherapy.
100
101 **Results**
102 **The AML cells infiltrated in skin can regenerate AML post-transplantation**
103 We have here studied extramedullary leukemia in skin by using an MLL-AF9$^+$ AML cell
104 transplantation-induced AML mouse model (**Figure 1A**). Post-symptomatic AML onset (day
105 21-30 post-transplantation), we detected the AML cell infiltration in the dorsal skin by
106 fluorescence-activated cell sorting (FACS) (**Figure 1B-1D**) and hematoxylin and eosin
107 staining (**Figure S1A**). The AML frequency was higher than that in the blood, but lower than
108 that in BM and spleen (**Figure 1B-1C**). There was no clear correlation between the AML
109 burden in skin and that in blood (**Figure S1B**). However, interestingly, the AML engraftment
110 level in the skin correlated with a faster AML onset (**Figure 1D**) but, not with the AML burden
111 in blood, pointing to a possible predicting value of AML cells in skin for AML progression.
112 Confocal imaging showed that these AML cells mainly resided at perivascular sites in the skin
113 (**Figure 1E**). The skin total cellularity was not affected (**Figure S1C**).
114 It is not known whether the AML cells infiltrated in skin contain LSCs capable to regenerate
115 leukemia, particularly after chemotherapy. We therefore analyzed the AML cells in the skin 3
116 days post-5-day treatment with cytarabine (Ara-C)/normal saline (NS) or at the endpoint when
117 the mice became moribund (**Figure 1F**). The AML engraftment in skin remained lower than
118 that in BM and spleen post-Ara-C (**Figure 1G, Figure S1D**), however, there was no clear
119 difference in the fraction of chemoresistant CD36$^+$ AML cells and colony-forming unit-in
120 culture (CFU-C) in the AML cells from different tissues (**Figure 1H-1I**).
121 To functionally assess the frequency of the AML-initiating LSCs in the skin and BM, we
122 sorted the AML cells from the primary recipient mice post-Ara-C treatment (100mg/Kg, daily)
123 and performed secondary transplantation into non-irradiated mice in limiting dilution at doses
124 of 10, 100, 1000 and 5000 cells per mouse (**Figure 1F**). The primary recipients treated with
125 NS showed clear severe symptoms at day 22-33 resulting in ethical endpoint with an estimated
126 median survival of 23.5 days. The median survival of the Ara-C-treated mice was 32 days
127 (**Figure 1J**). The AML cells were sorted at 2-3 days after the last injection of Ara-C or NS.
128 Notably, these AML cells in the skin could generate AML even at a low dose (10-100
129 cells/mouse) (**Figure 1J-1O**), as shown by the survival (**Figure 1J**), low platelet counts
130 (**Figure 1K**), splenomegaly (**Figure 1L**) and high AML engraftment in the BM at the endpoint

131 (**Figure 1M-1N)**. Extreme Limiting Dilution analysis (Hu and Smyth, 2009) revealed that the
132 frequency of residual AML-initiating LSCs in the skin (1/51) is similar to that in the BM (1/42)
133 post-Ara-C treatment, but seemed to be somewhat higher than that (1/92) from the nontreated
134 skin (**Figure 1O)**. Given the higher AML cell frequency in the BM and spleen, the % of the
135 AML-initiating LSCs and CFU-Cs in BM and spleen became higher than that in the skin
136 (**Figure S1E**, **Figure 1P**). These data demonstrate the leukemia-initiating capacity of the AML
137 cells in the skin tissue under steady-state and after chemotherapy, indicating their potential
138 impact on AML relapse.
139

140 **Skin harbors Ebf2$^+$ and Ebf2$^-$ MPC subsets with similar immunophenotype to BM MSCs**

141 To understand how the leukemic cells were maintained in the skin tissue, we explored the
142 role of the extramedullary microenvironment in the skin using a similar approach as was used
143 for characterizing the BM niche. BM MSCs have been shown to be involved in AML
144 progression in mice (Xiao et al., 2018b). They are defined by a phenotype of lacking expression
145 of CD44, hematopoietic (CD45/TER119) and endothelial (CD31) cell markers, but positive for
146 PDGFRa/CD140a, SCA1 and CD51 (Morikawa et al., 2009; Pinho et al., 2013; Schepers et al.,
147 2013; Xiao et al., 2018a; Xiao et al., 2018b). The primitive MSCs in mouse BM can be
148 identified by Ebf2 expression (Qian et al., 2013) and can generate MSCs that lack Ebf2 (Xiao
149 et al., 2018b). However, the phenotype of native skin MSCs remains unknown. The question
150 is whether the cells with similar features exist in skin and play a role in the AML cell
151 maintenance under steady-state and following chemotherapy. To answer this, we first
152 characterized mesenchymal stem and progenitors in the skin by using the *Ebf2-Egfp* reporter
153 mice. Similar to BM, a fraction of CD45$^-$TER119$^-$CD31$^-$ skin stromal cells expressed Ebf2
154 (**Figure 2A**). The Ebf2$^+$ cells accounted for about 2% and 5% of total live cells and CD45$^-$
155 TER119$^-$CD31$^-$ stromal cells, respectively (**Figure 2B-2C**). Phenotypically, skin Ebf2$^+$ cells
156 highly expressed PDGFRa/CD140a and SCA1 (PαS) whereas about 41% of the Ebf2$^-$ cells
157 were PαS cells (**Figure 2D**).
158 Functionally, both the Ebf2$^+$ and Ebf2$^-$ cells contained CFU-Fs, a colony-forming unit
159 characteristic for MSCs (**Figure 2E, Figure S2A**). The CFU-Fs in the Ebf2$^+$ cells were
160 generated exclusively by the SCA1$^+$ population (**Figure 2F**). Both Ebf2$^+$ and Ebf2$^-$PαS cell
161 populations showed similar proliferation kinetics after passage 5-6 (**Figure S2B**) and were able
162 to differentiate towards osteogenic and adipogenic lineages *in vitro* albeit to a different degree
163 (**Figure S2C-S2D**). However, they failed to differentiate into chondrocytes in either monolayer

164 or micromass pellet culture in which condition BM MSCs could differentiate into chondrocytes
165 (**Figure S2E**). These data indicate that the Ebf2$^+$ and Ebf2$^-$PαS cells in mouse skin may
166 represent bipotential MPCs although they have the same immunophenotype as BM MSCs.
167

168 **Single-cell assay confirms osteo-adipo bipotentials of skin Ebf2$^+$ and Ebf2$^-$PαS cells**

169 To validate the identity of the skin stromal subsets, we characterized these cells at single
170 cell level. Limiting dilution experiment revealed that the CFU-F frequency in both skin Ebf2$^+$
171 and Ebf2$^-$PαS fractions was as high as 1 in 4 (**Figure 2G, 2I**). Of 13 randomly selected CFU-
172 Fs from single Ebf2$^+$ cells, 9 (69.2 %) showed both osteogenic and adipogenic differentiation
173 potency although to different degrees (**Figure 2H, 2K**). However, only 45.4% (5 of 11) of the
174 Ebf2$^-$PαS cells showed bi-lineage potency toward osteoblasts and adipocytes (**Figure 2J-2K**).
175 The chondrogenic potency, however, was not evaluated at single cell level since none of these
176 cell subsets differentiated into chondrocytes at the bulk level. The self-renewal capacity of the
177 Ebf2$^+$ and Ebf2$^-$ cells was evaluated by serially replating of single CFU-F derived from the
178 single sorted cells. Eleven out of 25 CFU-Fs initially generated by single Ebf2$^+$ cells could be
179 serially replated for beyond 10 passages (**Figure 2L**). Meanwhile, only 4 in 20 CFU-F clones
180 derived from Ebf2$^-$PαS cells could be serially replated for over 10 passages (**Figure 2L**),
181 indicating a limited self-renewal capacity of the Ebf2$^-$PαS cells. These data further support the
182 notion that the skin Ebf2$^+$ and Ebf2$^-$PαS cells are enriched with osteo-adipogenic MPCs.
183

184 **Skin Ebf2$^+$ cells are mainly located at perivascular sites**

185 Similar to that in mouse BM, the skin Ebf2$^+$ cells did not express endothelial cell marker CD31
186 (**Figure S3A**). However, the Ebf2$^+$ cells highly expressed PDGFRb/CD140b, a marker
187 expressed in pericytes (Armulik et al., 2011) and niche-forming perivascular cells in BM
188 (Kusumbe et al., 2016) (**Figure S3B**), pointing to a pericyte phenotype. Confocal imaging
189 illustrated that the majority of the Ebf2$^+$ cells were adjacent to the endothelial cells in the skin
190 (**Figure 3A-3B**, **Figure S3C**). Some scattered Ebf2$^+$ cells were also found in dermal panniculus
191 carnosus, a layer of striated muscle (**Figure 3A**). Approximately 55% and 41% of the Ebf2$^+$
192 cells were positive for the pericyte marker NG2, respectively (**Figure S3D, S3F**), and 81% of
193 them expressed α-smooth muscle actin (SMA) (**Figure S3E-S3F**), reported to mark pericytes
194 in BM (Baryawno et al., 2019). Altogether, these data suggest a perivascular origin and
195 heterogeneity of the skin Ebf2$^+$ cells.
196

197 **The Ebf2$^+$ cells in skin contribute to the mesenchymal cell turnover**

198 To understand how mesenchymal cell niche in the skin is maintained, we determined the
199 physiological contribution of the Ebf2$^+$ stromal cells to the niche formation by lineage-tracing
200 using Tg*Ebf2-Egfp xCre^{ERT2}* X *Rosa26-tomato* mice (**Figure 3C**). This mouse model allowed
201 us to track the fates of the Ebf2$^+$ cells *in vivo* since the Ebf2$^+$ cells express GFP and their
202 progeny is marked by Tomato after tamoxifen (TAM) injection. About 15% of total Ebf2$^+$ cells
203 were Tomato$^+$(Ebf2$^+$Tomato$^+$) cells at 3 months after TAM induction (**Figure S4A-S4B**). The
204 Ebf2$^+$Tomato$^+$ cells could generate Ebf2$^-$PαS MPCs and more mature CD45$^-$TER119$^-$CD31$^-$
205 CD44$^-$CD140a$^+$SCA1$^-$ stromal cells (**Figure 3D-3E**), indicating the important role of the Ebf2$^+$
206 cells in maintaining the mesenchymal cell compartment in the skin.

207 The fraction of the Ebf2$^+$Tomato$^+$ cells within stromal cells remained constant up to 12
208 months post-TAM induction (**Figure 3E**), which is likely attributed to their self-renewal ability.
209 However, the Ebf2$^-$Tomato$^+$ cells which were produced by the Ebf2$^+$Tomato$^+$ cells increased
210 from 11% at 3 months to 21% at 6 months post-TAM injection, then remained stable (**Figure**
211 **3E**). Within the newly generated Ebf2$^-$Tomato$^+$ cells, the majority were PαS MPCs and about
212 5% were the CD140a$^+$SCA1$^-$ cells (**Figure 3F**). Inversely, within the total PαS MPCs, only
213 0.5% were Ebf2$^+$Tomato$^+$ cells and 30% were the newly generated Ebf2$^-$Tomato$^+$ PαS cells at
214 6 months post-TAM (**Figure S4C-S4E**). These data suggest a substantial contribution of the
215 Ebf2$^+$ MPCs to generating the Ebf2$^-$Tomato$^+$PαS MPCs while maintaining the Ebf2$^+$ cell pool.

216 Similar to the Ebf2$^+$ cells, the Ebf2$^-$Tomato$^+$ cells were mainly distributed in the lower
217 dermis and adjacent to CD31$^+$ endothelial cells (**Figure 3G**). However, they lacked NG2
218 expression (**Figure S4F**). Only 19% and 28% of the Ebf2$^-$Tomato$^+$ cells expressed NESTIN
219 and α-SMA, respectively (**Figure S4G-S4I**).

220 Altogether, skin harbors Ebf2$^+$ and Ebf2$^-$PαS MPCs with a similar phenotype as BM MSCs.
221 The Ebf2$^+$ MPCs reside at the top of the developmental hierarchy and contribute to
222 mesenchymal cell generation in the skin.

223

224 **Skin MPCs play a role in maintaining normal hematopoietic and AML cells *in vitro***

225 Identification of the skin MPC populations made it possible to analyze their potential role
226 in the maintenance of AML cells. We first evaluated the function of skin MPC subsets in
227 supporting normal hematopoietic stem cells (HSCs) in a co-culture system and compared to
228 BM MSCs (**Figure S5A**). Similar to their BM counterparts, both skin Ebf2$^+$ and Ebf2$^-$PαS
229 MPCs were able to maintain HSC activities**,** indicated by similar numbers of CFU-Cs generated

230 from the Lineage$^-$ SCA1$^+$KIT$^+$(LSK)CD150$^+$ cells after the co-culture with skin MPCs or BM
231 MSCs (**Figure S5B-S5C**). Further, similar cobblestone area forming cells (CAFCs) were
232 generated from the BM LSK cells co-cultured with the skin MPCs or BM MSCs (**Figure S5D-**
233 **S5E**). The BM Ebf2$^-$PαS cells displayed better capacity in supporting CAFC formation from
234 the LSK cells than the BM Ebf2$^+$ MSCs (**Figure S5F**). Altogether, these data indicated that
235 skin MPCs possessed similar hematopoiesis supportive function as BM MSCs.
236 To assess the role of skin MPCs in supporting AML LSC growth, we next performed CAFC
237 assay of MLL-AF9$^+$ AML cells (**Figure 4A**). Like BM MSCs, skin MPC subsets could support
238 CAFC formation from the AML cells, but to a lesser degree than the BM Ebf2$^-$PαS cells
239 (**Figure 4B-4C**).
240 Increasing evidence suggests that BM stromal cells may protect leukemia cells from
241 cytostatic drugs (Alonso et al., 2015; Iwamoto et al., 2007; Jin et al., 2008; Xu et al., 2016;
242 Zhang et al., 2013). However, it is not known if extramedullary stromal cells have similar
243 functions. We then tested the chemoprotective function of skin MPCs by CAFC assay. We
244 administered Ara-C 2 days after seeding the MLL-AF9$^+$ AML cells to the MPCs to allow for
245 efficient cell-cell interactions (**Figure 4A**). Both skin Ebf2$^+$ and Ebf2$^-$PαS cells could protect
246 the AML LSCs from Ara-C treatment, demonstrated by the persistence of residual CAFCs after
247 Ara-C treatment, in striking contrast to the efficient killing of the AML cells cultured alone
248 (**Figure 4D-4E**). No difference in the frequency of KIT$^+$ AML cells, representing AML LSCs
249 (Somervaille and Cleary, 2006) was observed among all the co-cultures (**Figure 4F**). However,
250 the numbers of the residual KIT$^+$ LSCs were significantly increased in the co-cultures with the
251 stromal cells compared to the monoculture post-Ara-C treatment (**Figure 4G**). CD36 was
252 reported to be a marker for chemoresistant leukemic cells (Farge et al., 2017; Landberg et al.,
253 2018; Ye et al., 2016). Post-Ara-C, the CD36$^+$ AML cells were selectively enriched in all the
254 co-cultures except that with skin Ebf2$^-$PαS MPCs (**Figure 4H**), however, only in the culture
255 with skin MPC subsets, significant more CD36$^+$ AML cells were retained (**Figure 4I**). These
256 data indicate a previously unrecognized role of skin MPCs in AML LSC maintenance and
257 protection.

258

259 **The altered mesenchymal niches in the skin during AML development**

260 Niche-remodeling in BM has been considered as one of the mechanisms contributing to
261 leukemia progression (Ahsberg et al., 2020; Cai et al., 2022; Duarte et al., 2018; Xiao et al.,
262 2018b). By confocal imaging, we observed the perivascular location of the AML cells (**Figure**

263 **1E**) and the localization adjacent to the skin Ebf2/GFP$^+$ MPCs (**Figure 4J**). We then evaluated
264 whether the skin cellular niches were remodeled by the AML cells. The proportion of Ebf2$^+$
265 MPCs but not the Ebf2$^-$PαS cells in the skin stromal cells were reduced post-symptomatic onset
266 of AML (**Figure 4K-4N**). While this finding seems to be contrary to our previous observation
267 of BM MSC increase in AML mouse BM, it is somewhat consistent with the reduced PαS cell
268 fraction within the Ebf2$^+$ cells in the AML mouse BM (Xiao et al., 2018b). In addition, while
269 the total CD31$^+$ endothelial cells were unaltered, as observed in BM (Xiao et al., 2018b), the
270 CD31$^+$SCA1$^+$ arteriolar endothelial cells were significantly increased (**Figure 4O-4P**),
271 indicating an increase of arterioles in dorsal skin during AML development.
272
273 **Molecular evidence for the role of skin MPCs in hematopoiesis and AML**
274 To investigate the molecular mechanisms behind the hematopoiesis-supportive function of
275 the skin MPCs, we performed RNA sequencing on the freshly sorted skin Ebf2$^+$ and Ebf2$^-$PαS
276 MPCs. This revealed a distinct transcriptional profile of skin MPCs and BM MSCs with 1150
277 and 816 genes differentially expressed between skin Ebf2$^+$ and Ebf2$^-$PαS MPCs compared to
278 BM MSCs, respectively (**Figure 5A**). However, only 135 genes were differentially expressed
279 between the skin Ebf2$^+$ and Ebf2$^-$PαS cells. Among them, the genes associated with TNFα
280 signaling, angiogenesis and epithelial to mesenchymal transition were upregulated while the
281 cell proliferation genes were downregulated in the more primitive Ebf2$^+$ cells (**Figure 5B**). We
282 then compared skin MPC pool (Ebf2$^+$ and Ebf2$^-$PαS) with BM MSCs. The genes related to
283 skin tissue maintenance (*Krt14*, *Krt19*) and adipogenesis (*Fabp4*) were upregulated in the skin
284 MPCs (**Figure 5C-5D**), showing tissue origin-related characteristics of these cells. Consistent
285 with the limited chondrogenic differentiation capacity of skin MPCs (**Figure S2C-S2D**), the
286 genes associated with chondrogenesis were downregulated in the cells (**Figure 5E**).
287 Conversely, skin MPCs were enriched with genes related to fatty acid metabolism and
288 oxidative phosphorylation indicating a distinct metabolic profile between the skin and BM
289 MSCs (**Figure 5D-5E**). Furthermore, the genes related to inflammatory response were
290 enriched in the skin MPCs relative to BM MSCs (**Figure 5E-5F**), indicating a possible pro-
291 inflammatory phenotype of skin MPCs.
292
293 Notably, there was no overall significant difference in the hematopoiesis supportive gene
294 expression between the skin MPCs and BM MSCs (**Figure 5G**). The findings were confirmed
295 by Q-PCR of the genes in these freshly sorted cells (**Figure 5H**). Similar to BM MSCs, both

296 skin MPC subsets expressed *Cxcl12*, *Kitl*, *Jag1, Lama4* and *Angptl1,* all of which are known
297 to be critical for hematopoiesis maintenance and regeneration (Arai et al., 2004; Calvi et al.,
298 2003; Greenbaum et al., 2013; Gu et al., 2003; Omatsu et al., 2010; Poulos et al., 2013; Susek
299 et al., 2018; Thoren et al., 2008). The expressions of *Kitl*, *Jag1* and *Lama4* were even
300 significantly higher in skin Ebf2^{+} and Ebf2^{-}PαS cells than that in BM MSCs. Moreover, the
301 expression of *Spp1,* a negative regulator of HSC expansion (Stier et al., 2005) was lower in
302 skin MPCs than that in BM MSCs (**Figure 5C, 5H**).These data provide molecular evidence for
303 the supportive function of skin MPCs for HSCs and AML LSCs.
304

305 **Enhanced mitochondrial transfer from skin MPCs to AML cells associated with**
306 **increased chemoprotection of AML cells**

307 To reveal the mechanisms underlying the function of skin MPCs in maintaining and
308 protecting AML LSCs, we examined the metabolic activity of skin MPCs in supporting AML
309 cells since the genes related to oxidative phosphorylation and fatty acid metabolism are
310 enriched in the skin MPCs. Mitochondria transfer has been reported as one of the protective
311 mechanisms during chemotherapy in leukemias by providing energy support and anti-oxidant
312 machinery to counteract oxidative stress induced by chemotherapy (Batsivari et al., 2020; Cai
313 et al., 2022; Marlein et al., 2017; Moschoi et al., 2016). Consistent with their gene expression
314 profile, our FACS analysis showed increased mitochondrial mass of skin MPCs compared to
315 BM MSCs (**Figure 6A-6B**). Further, in a co-culture with mitochondria-prelabeled skin MPCs
316 (**Figure 6C**), we detected enhanced mitochondrial transfer from skin MPCs to the AML cells
317 compared to BM MSCs (**Figure 6D-6E**). Correspondingly, the AML cells co-cultured with
318 skin MPCs showed lower ROS levels and higher viability during Ara-C treatment (**Figure 6F-**
319 **6G**). The mitochondrial transfer and chemoprotection could be partially reversed by the
320 treatment with microtubule inhibitor nocodazole and colchicine in the co-cultures (**Figure 6H-**
321 **6J**). Similar to a previous report (Moschoi et al., 2016), the mitochondrial transfer seemed to
322 be leukemia-specific since little or no mitochondrial transfer from skin MPCs to normal HSPCs
323 (LSK BM cells) was detected in the co-cultures (**Figure 6K-6L**). Together, these data indicated
324 that skin MPCs could maintain AML LSCs and protect them from Ara-C treatment *in vitro*
325 partially by reducing oxidative stress.

326 ***Lama4* loss in skin MPCs enhanced AML LSC proliferation and chemoprotection *in vitro***

327 *Lama4* was highly expressed in skin MPCs (**Figure 5H**) and we have found that *Lama4*
328 loss in mice promoted AML LSC proliferation, chemoresistance, and relapse (Cai et al., 2022).

329 This has tempted us to test the impact of *Lama4* deletion in skin MPCs on AML LSC growth
330 (**Figure 6M**). We observed increased AML cell proliferation and chemoresistance to Ara-C at
331 24h post-co-culture with *Lama4*$^{-/-}$ skin MPCs (**Figure 6N**). Further CAFC assay indicated that
332 *Lama4*$^{-/-}$ skin MPCs promoted AML LSC proliferation and chemoresistance to Ara-C (**Figure**
333 **6O**), suggesting a suppressive impact of *Lama4* expression in skin MPCs on AML cell growth
334 and chemoresistance.
335
336 **The increased chemoresistant AML cells in *Lama4*$^{-/-}$ mouse skin post-Ara-C treatment**
337 To further explore the molecular mechanism involving in the role of the extramedullary
338 niche in the skin for maintaining residual AML cells after chemotherapy, we here took
339 advantage of *Lama4*$^{-/-}$ mice where AML progression and relapse are accelerated (Cai et al.,
340 2022). To facilitate imaging of engrafted AML cells, DsRed-expressing MLL-AF9 AML cells
341 were transplanted in sublethally irradiated *Lama4*$^{+/+}$ and *Lama4*$^{-/-}$ mice (**Figure 7A**). The mice
342 were treated with either Ara-C or NS for 5 days at day 15 post-AML transplantation.
343 Interestingly, one day post-Ara-C treatment, confocal imaging illustrated more AML cells in
344 *Lama4*$^{-/-}$ mouse skin, compared to that in *Lama4*$^{+/+}$ mice following either NS or Ara-C
345 treatment (**Figure 7B**). However, such a difference was not detected by FACS while there was
346 a clear reduction of the AML cells in the PB and skin after Ara-C treatment (**Figure 7C**). It is
347 possible that some of the remaining AML cells were lost during enzymatic digestion of the
348 skin for FACS whereas confocal imaging was performed on the tissue fixed directly after
349 dissecting. It is important to note that the chemoresistant CD36^{+} AML cells (Farge et al., 2017;
350 Ye et al., 2016), not KIT^{+} cells were enriched in *Lama4*$^{-/-}$ mouse skin post-Ara-C treatment
351 (**Figure 7D**), which was not observed in the BM (Cai et al., 2022). It is worth mentioning that
352 there was no homing preference of the AML cells to *Lama4*$^{-/-}$ skin and BM compared to that
353 in *Lama4*$^{+/+}$ mice (**Figure 7E-7G**), suggesting that the observation of more AML cells in
354 *Lama4*$^{-/-}$ mouse skin was not related to the initial homing of the AML cells. Further, the AML
355 cell homing to skin and BM was similar at 3 hours post-transplantation (**Figure 7H**), pointing
356 towards a possibility that the skin tissue may act as an independent AML niche from the BM.
357
358 To functionally evaluate AML-initiating LSCs, we performed serial transplantation with
359 limited cell doses (10, 100, 1000 cells/mouse) and CFU-C assay post-Ara-C treatment (**Figure**
360 **8A**). Extreme limiting dilution analysis (Hu and Smyth, 2009) indicated no significant
361 difference in the frequency of AML-initiating LSCs within the residual AML cells from
362 *Lama4*$^{+/+}$ and *Lama4*$^{-/-}$ mouse skin (**Figure 8B-8C**). However, due to a relatively higher % of

363 total AML cells in the donor *Lama4*$^{-/-}$ mouse skin than that in the *Lama4*$^{+/+}$ mice (**Figure 8D**),
364 the calculated % of the AML-initiating LSCs and AML CFU-Cs in the *Lama4*$^{-/-}$ skin appeared
365 to be higher than that in the *Lama4*$^{+/+}$ skin (**Figure 8E**). These data suggest that *Lama4*
366 expression in skin mesenchymal niche plays a role in maintaining the chemosensitivity of AML
367 cells in the skin to Ara-C.
368
369 **Discussion**

370 Leukemia cutis is commonly observed in patients with monocytic AML and pediatric
371 patients with congenital leukemia are prone to develop leukemia cutis (Parsi et al., 2020).
372 Despite its association with a poor prognosis (Bakst et al., 2011; Gouache et al., 2018; Wang
373 et al., 2019), the pathogenesis and impact of leukemia cutis on AML relapse remain largely
374 unknown. We here have demonstrated in a transplantation-induced MLL-AF9 AML mouse
375 model that the AML cells infiltrate in mouse skin, similar to leukemia cutis observed in patients
376 with AML. Importantly, these skin-derived AML cells can efficiently regenerate AML post-
377 transplantation even at a low dose (10 cells per mouse), indicating their high capacity in
378 regenerating AML and pointing to a possible involvement of these leukemic cells in the relapse
379 of AML.
380 Currently, little is known about the leukemia microenvironment or niche in the skin, which
381 has limited our understanding of how leukemia cutis is maintained. We report that skin harbors
382 two MPC subsets distinguished by Ebf2 expression, the Ebf2^{+} and Ebf2^{-}PαS cells, sharing a
383 similar phenotype with BM MSCs (Morikawa et al., 2009; Qian et al., 2013; Qian et al., 2012).
384 The skin Ebf2^{+} MPCs co-express pericyte markers like CD140b/PDGFRb and α-SMA and
385 show pericyte phenotype. The adjacent localization of the Ebf2^{+} cells to the AML cells in skin
386 indicated a possibility that these cells act as a niche component for maintaining AML cells.
387 This notion is supported by another important finding in this study that skin MPCs, similar to
388 BM MSCs, show a supportive/protective function for AML LSCs. During AML progression,
389 the skin mesenchymal cell niches are also altered with increased arteriolar endothelial cells and
390 reduced Ebf2^{+}, but not Ebf2^{-}PαS MPCs after symptomatic AML onset. The niche-remodeling
391 might in turn further promote AML progression since Ebf2^{+} cell deletion in mice accelerated
392 AML development, as reported (Xiao et al., 2018b).
393
394 We have here attempted to address the potential mechanisms mediating the supportive role
395 of skin MPCs. It is most likely that multiple mechanisms are involved in the AML protective

396 role of skin MPCs. Mitochondrial transfer from stromal cells to leukemic cells has been
397 reported to be one of the mechanisms to protect leukemic cells to survive from chemotherapy
398 by providing an antioxidant system to counteract the therapy-induced oxidative stress (Forte et
399 al., 2020). We find the increased mitochondrial mass in skin MPCs and enhanced
400 mitochondrial transfer from skin MPCs to the AML cells during chemotherapy, compared to
401 that in BM MSCs. Blocking mitochondrial transfer by microtubule inhibitors in the co-culture
402 could compromise the protective effects of skin MPCs. These data suggest that skin MPCs may
403 protect the AML cells by providing metabolic support via mitochondrial transfer. This notion
404 was further supported by the enrichment of genes related to oxidative phosphorylation, fatty
405 acid metabolism and glycolysis in skin MPCs. Furthermore, the skin MPCs express a higher
406 level of *Lama4*, *Kitl* and *Jag1* than BM MSCs, which are known to be important for normal
407 hematopoiesis maintenance and leukemic cell proliferation (Cai et al., 2022; Poulos et al., 2013;
408 Somervaille and Cleary, 2006; Thoren et al., 2008). Our data indicate that *Lama4* expression
409 in skin MPCs may have an impact on AML LSC chemosensitivity since *Lama4* deletion in
410 skin MPCs led to enhanced proliferation and chemoprotection of AML LSCs. More work is
411 required for assessing the potential impact of other niche factors like *Kitl, Jag1* and *Angptl*. In
412 addition, the upregulation of inflammatory cytokines including interferon, *Il6*, *Il18*, *Il4* and
413 *Cxcl10* in the skin MPCs points to another possible mechanism contributing to the AML
414 maintenance in the skin, as these cytokines affect leukemic/cancer cell growth (Madapura et
415 al., 2017; Manshouri et al., 2011; Pena-Martinez et al., 2018; Welner et al., 2015).
416 The origin of the AML cells in the skin remains an open question. In patients, leukemia cutis
417 is usually present concurrently with AML cell infiltration in BM. However, in some cases, it
418 may precede systemic involvement (Krooks and Weatherall, 2018). Therefore, it is unclear
419 whether the leukemic cells infiltrated in the skin originate from BM. We here find that the
420 AML engraftment in the skin does not correlate with that in the blood, suggesting AML cell
421 maintenance in the skin may not be dependent on the circulating AML cells although they were
422 initially derived from the injected AML cells. On the contrary, the AML burden in skin
423 inversely correlates with the time of AML symptomatic onset, which is in line with the
424 association of leukemia cutis with poor prognosis in patients with AML (Krooks and
425 Weatherall, 2018).

426 In summary, we here report that skin harbors primitive Ebf2^{+} MPCs and the downstream
427 Ebf2^{-} MPCs. These MPCs are colocalized with AML cells at perivascular sites during AML
428 development. The residual AML cells in the skin after chemotherapy can regenerate leukemia

429 post-transplantation, indicating the existence of AML LSCs in the skin. The skin MPCs can
430 provide metabolic support for AML cells to protect them from chemotherapy *in vitro*. We for
431 the first time provide evidence for the characteristics of skin mesenchymal cell niches and their
432 roles in AML LSC growth and chemotherapy response, as well as the impact of *Lama4*
433 expression in the niches on the chemoprotection of AML LSCs. These findings warrant future
434 studies on the role of skin mesenchymal niches in chemotherapy response and relapse of AML
435 patients.
436

437 **Methods**

438 **Mice**

439 *Ebf2-Egfp* reporter FVB/N mice (RRID:MGI:4421814) (Qian et al., 2013) at 8 to 14-week old
440 were used. Transgenic *Ebf2-Egfp*X*Ebf2-Cre*^{ERT2}X *Rosa26*^{loxp}*Stop*^{loxp}*-Tomato* mice were
441 generated by crossing *Ebf2-Egfp* with *Ebf2-Cre*^{ERT2}X*Rosa26*^{loxp}*Stop*^{loxp}*-Tomato* mice for
442 lineage tracing. To activate Cre, tamoxifen (TAM) (Sigma) was intraperitoneally injected at 3
443 mg/20g body weight for 3 times every second day (Xiao et al., 2018b). *Lama4*$^{-/-}$ C57BL/6 mice
444 were generated as described (Thyboll et al., 2002). All mice were maintained in specific-
445 pathogen-free conditions in the animal facility of Karolinska Institute. Animal procedures were
446 approved by local ethics committee (ethical number 15861-2018) at Karolinska Institute
447 (Stockholm, Sweden).
448

449 **Generation of MLL-AF9-induced AML mouse model**

450 AML mouse model was induced as previously described (Xiao et al., 2018b). Briefly, 250.000
451 MLL-AF9 expressing cells were intravenously injected into non-irradiated mice to generate
452 the AML mouse model. For detecting AML infiltration in dorsal skin tissue, 1x10^{6} of MLL-
453 AF9 previously generated in DsRed C57BL/6J transgenic mice (Hartwell et al., 2013) were
454 intravenously injected into sublethally irradiated (6 Gy) *Lama4*$^{+/+}$ and *Lama4*$^{-/-}$ mice, as
455 described (Cai et al., 2022). At day 15, the mice were treated intraperitoneally with Cytarabine
456 (Ara-C, Jena Bioscience) at the dose of 100mg/Kg or 700mg/kg body weight, daily for 5
457 consecutive days. For non-irradiated mice, the treatment started at day 20. The mice were
458 sacrificed one day after the last injection for AML engraftment analysis in peripheral blood
459 (PB), BM and dorsal skin by FACS. The distribution of residual AML cells in dorsal skin was
460 visualized by confocal imaging.

461

462 **Skin MPC isolation by FACS**

463 Mouse dorsal skin was minced and digested with 0.2% collagenase II (CLSII Worthington
464 Biochemicals) in PBS supplemented with 20% FBS for 60 minutes at 37°C. After washing
465 with PBS/20%FBS followed by PBS, the digested skin tissue was treated with 0.05% trypsin-
466 EDTA (GIBCO) for 10 to 15 minutes at 37°C. Cell suspension was spun down at 300 g for 10
467 minutes. Mononuclear cells were then incubated with FcR (CD16/32) antibody and stained
468 with CD45, TER119, CD31, CD44, CD140a, and SCA1 for 15 minutes at 2-8°C. Dead cells
469 were excluded by propidium iodide (PI) staining. For sorting native skin MPCs, hematopoietic
470 and endothelial populations were firstly excluded ($CD45^-TER119^-CD31^-$) and Ebf2 gate was
471 then defined based on Fluorescence Minus One (FMO) using skin mononuclear cells from a
472 non-transgenic mouse. Skin $Ebf2^+$ and $Ebf2^-$ cells were sorted on a FACS Aria III Sorp (BD
473 Biosciences, San Jose). See Table S1 for detailed antibody information.

474

475 **Serial transplantation**

476 To test the leukemia-initiating capacity of the AML cells infiltrated in skin tissue, the AML
477 $CD45.1^+$ cells were sorted from skin tissue of the mice that have developed AML post-AML
478 cell injection. The mice were treated with normal saline or Ara-C for 5 days at day 20-21 after
479 AML cell injection. The AML cells in skin were collected 2-3 days after the last injection,
480 sorted by FACS and transplanted into non-irradiated secondary C57BL/6J recipient mice via
481 tail vein at a dose of 10, 100. 1000 or 5000 cells per mouse. The AML development was
482 monitored by blood analysis using FACS and Sysmex as well as by assessing the general health
483 conditions. The survival rate of the mice was estimated based on the date when the mice were
484 found dead or in moribund status. Bones and blood were collected for determining AML
485 engraftment.

486

487 ***In vivo* lineage tracing**

488 This was performed as previously described (Xiao et al., 2018b). Dorsal skin from triple
489 transgenic *Ebf2-Egfp* x *Ebf2-Cre*^{ERT2} x *Rosa26*^{loxp}*Stop*^{loxp}- *Tomato* mice (Xiao et al., 2018b)
490 were collected at 3, 6 and 12 months after tamoxifen injection. Approximately, 1 x 1 cm of
491 dorsal skin tissue was fixed and embedded in OCT for whole mount immunofluorescence. For
492 evaluating the frequency of $Ebf2^+$ cells and their progeny ($Tomato^+$), 2 x 2 cm of dorsal skin
493 tissue was processed for skin MPC isolation by FACS (BD FACS Aria^{TM} III). For defining the
494 gates for GFP^+ and $Tomato^+$ cells, cells from bi-transgenic or single transgenic mouse were

495 used as FMO controls. After excluding dead cells by PI staining, the CD45$^-$TER119$^-$CD31$^-$
496 stromal cells were gated. Subsequently, the CD44$^-$ fractions were divided based on CD140a
497 and SCA1 expression.
498
499 **Skin MPC expansion and proliferation kinetics *in vitro***
500 For *in vitro* expansion, CFU-Fs from FACS-sorted skin Ebf2$^+$ and Ebf2$^-$PαS cells were
501 trypsinized with 0.05% trypsin-EDTA (GIBCO), collected, and plated to T-25 flasks at 400
502 cells /cm^2. Cells were then expanded in complete Dulbecco modified Eagle Medium (DMEM,
503 31966, GIBCO) containing 10% FBS, 10 mM HEPES (1 M), 100 U of penicillin / streptomycin,
504 and 10^{-4} M 2-Mercaptoethanol (M7522, Sigma) under hypoxic condition (1-2% O_2) until 80%-
505 90% confluence was reached. Proliferation rates of skin Ebf2$^+$ and Ebf2$^-$PαS cells were
506 evaluated by population doubling time (PDT) assays. PDT was calculated by dividing number
507 of days for culturing the cells with number of population doublings (PDs) using following
508 formula: PDT=Culture time (days)/PD where PD=log (NH/NI)/log2, NH is harvested cell
509 number and NI is initial cell number.
510
511 **Dorsal skin wholemount immunofluorescence staining**
512 Dorsal skin specimens were fixed in 4% PFA for 10 minutes followed by washing with PBS
513 prior to embedding in OCT-Compound (Sakura Tissue Tex®, 4583). For immunofluorescence
514 staining, 150 µm dorsal skin sections were first blocked with skim milk, fish skin gelatin
515 (G7765, Sigma) and Triton X-100 (T8787, Sigma) for 1hour at RT. To visualize Ebf2$^+$ cells in
516 mouse dorsal skin, the sections were incubated with anti-GFP, additionally stained with either
517 anti-mouse MECA32, CD31, NG2, NESTIN, or α-SMA antibodies. All stainings were
518 performed at 2-8°C overnight prior to washing with PBS and staining with secondary antibody.
519 Imaging was performed with confocal microscopy at Live Cell Imaging (LCI) facility after the
520 section was mounted in Mountant PermaFlour (TA-030-F19, Thermo). See Table S2 for
521 antibodies used for the confocal imaging.
522 Quantification of the Ebf2$^+$ or Ebf2/GFP$^-$Tomato$^+$ cells expressing NESTIN, NG2 or α-SMA
523 was performed with NIS-element AR-analysis ver 5.20.00 64-bit software (Nikon). From 100
524 µm section, 30-40 µm thickness was scanned with a confocal microscope to localize Ebf2$^+$ and
525 Ebf2$^+$ progenies (Ebf2/GFP$^-$Tomato$^+$ cells). Areas where Ebf2$^+$ and Ebf2/GFP$^-$Tomato$^+$ cells
526 were distributed were further imaged every 1-1.1 µm depth to obtain Region of interest (ROI).
527 Within ROI, positive expression of NESTIN, NG2 or α-SMA was defined based on control

528 sections stained with secondary antibodies only while GFP$^+$ signal was set based on samples
529 from non-GFP reporter mice. Three to 4 mice were included for the quantification.
530
531 **RNA sequencing**
532 Total RNA from freshly sorted skin Ebf2$^+$ cells, skin Ebf2$^-$ PαS cells and BM MSCs were
533 isolated with RNeasy Micro Kit (Qiagen) according to the manufacturer's protocol. cDNA was
534 prepared using SMART-Seq v4 Ultra Low Input RNA Kit for Sequencing (634898, Takara
535 Bio.). The cDNA quality was examined on Agilent TapeStation system (RRID:SCR_019547)
536 using a High Sensitivity D5000 ScreenTape (5067-5592, Agilent). One ng cDNA was used for
537 library preparation using *Nextera XT* DNA Library Preparation Kit (FC-131-1024 & FC-131-
538 1096, Illumina). The yield and quality of the amplified libraries were analyzed using Qubit by
539 Thermo Fisher and the Agilent Tapestation System. The indexed cDNA libraries were
540 sequenced on the Illumina 2000 or Nextseq 550 (Illumina, San Diego, CA) for a 75-cycle v2
541 sequencing run generating 75 bp single-end reads. About 7-20 million reads/sample were
542 obtained. Sample quality was assessed using FastQC (v0.11.8) and MultiQC (v1.7). Reads
543 were aligned to a reference built from Ensembl GRCm38 genome sequences using STAR
544 (RRID:SCR_004463, v2.6.1d). All mapped counts to each gene were further calculated by
545 FeatureCounts function from Subread package (Liao et al., 2013) installed in R. Genes with
546 Reads Per Kilobase of transcript per Million mapped reads (RPKM) values more than 0.1 were
547 considered as being actively transcribed and proceeded to the analysis of Differential Gene
548 Expression (DGE) (Mortazavi et al., 2008). The normalized read counts assigned to each
549 sample were generated by Deseq2 (RRID:SCR_015687). The differentially expressed genes
550 between the cell subsets were identified by adjusted *P* value ($p$adj < 0.05) using Benjamini-
551 Hochberg correction for multiple testing, together with thresholds at $\log_2$fold changes >1 (up-
552 regulated) or <-1 (down-regulated). For the Gene Set Enrichment Analysis (GSEA), the
553 normalized read counts were imported into the GSEA (v4.0.3) platform from Broad Institute
554 (http://www.broadinstitute.org/gsea/index.jsp), with three gene sets being tested, including
555 gene ontology (c5.all.v5.symbols.gmt), hallmark (h.all.v5.symbols.gmt) and KEGG
556 (c2.kegg.v5.symbols.gmt). Gene sets tested were considered to be statistically enriched when
557 the nominal *P* value < .01 and FDR < .25.
558
559
560 **Cobblestone area-forming cells (CAFC) assay using primary skin MPCs**

561 This was done as previously described (Cai et al., 2022; van Os et al., 2008). Briefly, 30.000
562 skin/BM MPCs were first plated into a 24-multiwell plate and maintained in complete
563 Dulbecco modified Eagle Medium (DMEM, 31966, GIBCO) containing 10% FBS, 10 mM
564 HEPES (1M), 100U of penicillin/streptomycin, and 10^{-4}M 2-Mercaptoethanol (M7522,Sigma)
565 under hypoxic condition (1% O_2). One day after, 150-300 MLL-AF9 or LSK cells were then
566 added on the stromal cells in Myelocult (M5300, Stem Cell Technologies) with 10^{-6} M
567 hydrocortisone (07904, Stem Cell Technologies), 1% penicillin streptomycin and 1ng/mL IL-
568 3 (R&D). The co-cultures were performed at 32°C in 5% CO_2 for 7-14 days. A CAFC was
569 defined as a cluster of more than 3 cells underneath the MSCs/MPCs. The CAFCs were
570 visualized and scored with inverted microscope (CKX41, Olympus) on day 7 and 10. The cells
571 were thereafter trypsinized and collected for FACS.
572
573 **Detection of reactive oxygen species (ROS) level and mitochondrial transfer**
574
575 This was done as recently described (Cai et al., 2022). The MSCs/MPCs or AML cells were
576 harvested and washed with PBS and incubated with 2 μM of H_2-DCFDA (C6827,
577 ThermoFisher) in DMEM at 37°C for 40 minutes to detect ROS level. The cells were then
578 rinsed twice with PBS and resuspended with 150 μL of PI (1:1000) in 5%FBS/PBS. ROS levels
579 were measured by FACS.
580
581 For mitochondrial transfer, MSCs or MPCs were stained with 100 nM MitoTracker™ red FM
582 (M22426, ThermoFisher) at 37°C for 40 min, according to the manufacturer's instructions. The
583 cells were washed twice with PBS, then incubated for 3-4 hours to remove unbound probe
584 before a final wash. Subsequently, 15,000-25,000 MLL-AF9 AML cells in Myelocult (M5300,
585 StemCell Technologies) were plated and co-cultured with prelabelled MSCs for 24 hours.
586 Mitochondrial transfer was quantified in AML cells ($CD45.1^+$) by FACS and analyzed for MFI
587 of the MitoTracker red.
588
589 **Multilineage differentiation assay**
590 This was done as described (Xiao et al., 2018b). The skin $Ebf2^+$, $Ebf2^-$ and $Ebf2^-$PαS cells were
591 expanded in culture and plated at 400 cells/cm^2 to each well of 24-well plate. For osteogenic
592 differentiation, cells were cultured with complete osteogenic medium mixed by human/mouse
593 StemXVivo osteogenic/adipogenic base medium (CCM007, R&D Systems) and mouse
594 StemXVivo ostegenic supplement (CCM009; R&D Systems) under normoxic condition for

595 14-21 days. Differentiation toward osteoblast was evaluated by 1% alizarin red S (A5533,
596 Sigma) staining after cell fixation with cold methanol. For adipogenic differentiation, the
597 culture was performed with DMEM containing 10% FBS, 10 mM HEPES (1M), 100U of
598 penicillin/streptomycin, 10^{-4} M 2-Mercaptoethanol (Sigma, M7522), 5 μg/mL insulin (I6634,
599 Sigma), 20 μM Indomethacin (I7378, Sigma), 0.0115 mg/mL isobutylmethylxanthine (I-7018,
600 Sigma), and 10^{-6} M dexamethasone (D2915, Sigma) for 2-3 weeks. Cells were first stained
601 with 500 μL of 2 μM of Bodipy™ 500/510 (Invitrogen, D3823) for imaging live adipocytes,
602 then fixed with 10% formalin and stained with 0.5% Oil Red O (O1391, Sigma). Chondrogenic
603 differentiation was induced in monolayer culture where cells were cultured in 37°C under
604 hypoxic condition (2% O_2) with DMEM high glucose containing 10 mM HEPES (1M), 100U
605 of penicillin/streptomycin, 10^{-4} M 2-Mercaptoethanol (M7522, Sigma), 2 mM pyruvate (P5280,
606 Sigma), 0.35 mM L-proline (P5607-25G, Sigma), ITS^{+3} (I-3146, Sigma), 5 μg/mL L-ascorbic
607 acid 2-phosphate (A7506, Sigma), 10^{-7} M dexamethasone (D2915, Sigma), and 10 ng/mL TGF-
608 β3 (100-36E, Peprotech). To assess chondrogenic differentiation, toluidine blue (T3260, Sigma)
609 (pH 2.0 to 2.5) was used to stain proteoglycan. Images were then taken under inverted
610 microscope (CKX41, Olympus).
611

612 ***In vitro* chondrogenic induction in micromass pellet**

613 After *in vitro* expansion, $2.5x10^5$ of BM MSCs or skin $Ebf2^+$ or skin $Ebf2^-$PαS MPCs were
614 collected in 15mL tube and spun down at 300 g for 7 minutes. After removal of supernatant,
615 500 μM of chondrogenic medium consisting of DMEM high glucose with 10 mM HEPES,
616 100U of penicillin/streptomycin, 10^{-4} M 2-Mercaptoethanol (M7522, Sigma), 2 mM pyruvate
617 (P5280, Sigma), 0.35 mM L-proline (P5607-25G, Sigma), ITS^{+3} (I-3146, Sigma), 5 μg/mL L-
618 ascorbic acid 2-phosphate (A7506, Sigma), 10^{-7} M dexamethasone (D2915, Sigma,), and 10
619 ng/mL TGF-β3 (100-36E, Peprotech) were added. The chondrogenic induction was performed
620 in 37°C under hypoxic condition (2% O_2). Every 2-3 days, the medium was replaced until day
621 28. For evaluating the chondrogenic induction, the micromass pellets were washed with PBS
622 prior to being fixed in 4% PFA for 2 days. After dehydration with 70% ethanol, the pellets
623 were stained with toluidine blue (T3260, Sigma) at pH 2.0 to 2.5 for 15–30 minutes. Thereafter,
624 the stained pellets were washed with 70% ethanol and embedded in OCT-compound (4583,
625 Sakura Tissue Tex®). To visualize the formation of proteoglycan, the embedded pellet was cut

626 to 10μm, mounted and observed by an inverted microscope (Axio Observer.Z1, Zeis). Images
627 were processed with Zen software (Carl Zeiss Microscopy, GmbH 2011).
628
629 **LIN$^-$SCA1$^+$KIT$^+$ (LSK) CD150$^+$ cell isolation**
630 The LSKCD150$^+$ HSCs were isolated from femurs and tibias of young adult mice, as described
631 (Xiao et al., 2018a). See Table S1 for antibody detail information.
632
633 **Co-culture of skin MPCs with LSKCD150$^+$ cells and colony-forming unit in culture**
634 **(CFU-C) assay**
635 Twenty-five thousand (25,000) expanded Ebf2$^+$ or Ebf2$^-$PαS MPCs from skin and BM at
636 passage 4-13 were plated into each well of a 12-well plate and maintained in complete
637 Dulbecco modified Eagle Medium (DMEM, 31966, GIBCO) containing 10% FBS, 10 mM
638 HEPES (1M), 100U of penicillin/streptomycin and 10^{-4} M 2-Mercaptoethanol (M7522, Sigma)
639 under hypoxic condition (2% O_2) for 24h prior co-culture. The co-cultures were started by
640 plating 2000 sorted LSKCD150$^+$ to each well in Myelocult medium (M5300, Stem Cell
641 Technologies) supplemented with 10^{-6} M hydrocortisone (74142, Stem Cell Technologies) and
642 1% penicillin streptomycin. After a 3-day co-culture in 5% CO_2 at 37°C, the medium
643 containing hematopoietic cells and trypsinized cells were collected for FACS analysis and
644 CFU-C assay in Methylcellulose M3434 (Stem Cell Technologies). After 10 days of culture at
645 37°C in 5% CO_2, the CFU-Cs were stained with 2,7-diaminofluorene (DAF staining) and scored
646 with an inverted microscope (CKX41, Olympus). A cell cluster with a minimum of 50 cells is
647 defined as one colony. Colonies with DAF staining were defined as erythrocytes-containing
648 colonies including CFU-GME and BFU-E, as performed (McGuckin et al., 2003; Xiao et al.,
649 2018a).
650
651 **Statistical analysis**
652 Unless mentioned, either unpaired t-test or Mann-Whitney test was used to determine the
653 difference between the groups or cell subsets. All statistical tests were performed with
654 GraphPad Prism 8 software (RRID: SCR_002798) with $P<0.05$ considered statistically
655 significant.
656 **Online supplemental material**
657
658 Fig. S1 shows AML cell distribution, absolute numbers in skin, BM, spleen and blood from
659 AML mice under steady state and post-chemotherapy. Fig. S2 illustrates *in vitro* expansion and

660 differentiation of the Skin Ebf2$^+$ and Ebf2$^-$ PαS cell subsets. Fig. S3 provides additional
661 evidence for the perivascular location and expression of α-SMA and NG2 of skin Ebf2$^+$
662 cells. Fig. S4 shows additional data from lineage-tracing studies suggesting that skin Ebf2$^+$
663 cells generated Ebf2$^-$ cells while maintaining themselves *in vivo*. Fig. S5 shows the data from
664 in vitro co-culture experiments indicating that skin MPCs have a similar hematopoiesis
665 supportive function to BM MSCs.
666

667 **Data availability**

668 The RNA sequencing data in Fig. 5 are available at GEO under accession number GSE167562.
669 All other data are available in the article or upon reasonable request to the corresponding author.
670

671 **Acknowledgements**

672 We thank Tina Jacob, Karl Annusver and Alexandra Are at Department of Cell and Molecular
673 Biology, Karolinska Institute, Sweden for valuable advice and technical discussion. We thank
674 Alexandre Piccini, Yuanyuan Zhang and Andranik Durguryan in our group for technical help
675 for the cell culture. We also thank Prof. Marja Ekblom, Lund University for her scientific input.
676 This study was supported by the Swedish Research Council (2019-01361,2022-01228),
677 Swedish Childhood Cancer Society (PR2015-0142, FoAss13/015, PR2017/0154, PR2020-
678 0166), Swedish Cancer Society (CAN2017/774, 19 0092 SIA and 20 1222PjF), Åke Olsson
679 foundation, Radiumhemmets Forskningsfonder (151241, 171162, 191253) and Karolinska
680 Institute Wallenberg Institute for Regenerative Medicine, Karolinska Institute doctoral
681 education (KID) funding (2-1293/2014, 2021-00480), Stiftelsen Clas Groschinskys
682 Minnesfond (ref:M16 50), Cancer Research KI (Karolinska Institute) and Incyte Biosciences
683 Nordic to H.Q., and the Swedish Research Council (2018-02963) and Swedish Cancer Society
684 (CAN 2018/793) to MK (Kasper). FACS analysis and cell sorting were performed at MedH
685 Flow Cytometry core facility (Karolinska Institute), supported by KI/SLL. The confocal
686 images were obtained at the LCI facility/Nikon Center of Excellence, Karolinska Institute,
687 supported by grants from the Knut and Alice Wallenberg Foundation, the Swedish Research
688 Council, KI infrastructure, Centre for Innovative Medicine and Jonasson center at the Royal
689 Institute of Technology. All major computations were performed on resources provided by the
690 Swedish National Infrastructure for Computing (SNIC)_through Uppsala Multidisciplinary
691 Center for Advanced Computational Science (UPPMAX) under Project sens2018540. We also

692 would like to thank the core facility at NEO, BEA, Bioinformatics and Expression Analysis,
693 which is supported by the board of research at the Karolinska Institute and the research
694 committee at the Karolinska Hospital.
695

696 **Author contributions**

697 LS has substantially participated in designing, performing experiments, collecting and
698 analyzing data and manuscript writing. HC, EL, PX, MK(Kondo), XS, LT, AM and ASJ
699 performed experiments, collected data and assisted with data analysis and manuscript-editing.
700 MK (Kasper) provided scientific input and assistance with confocal imaging of skin tissues.
701 MJ provided the DsRed-expressing MLL-AF9 AML cells and scientific input on the
702 manuscript. KT provided Lama4$^{-/-}$ mouse models and scientific input. HQ designed, performed
703 experiments, collected and analyzed data, wrote the manuscript. All authors have approved the
704 final version of the manuscript.

705 **Conflict of interest:** All authors declare no competing financial interest regarding this study.

706

707 **References**

708

709 Ahsberg, J., P. Xiao, K. Okuyama, R. Somasundaram, T. Strid, H. Qian, and M. Sigvardsson.
710 2020. Progression of progenitor B-cell leukemia is associated with alterations of
711 the bone marrow micro-environment. *Haematologica* 105:e102-e106.
712 Alonso, S., M. Su, J.W. Jones, S. Ganguly, M.A. Kane, R.J. Jones, and G. Ghiaur. 2015. Human
713 bone marrow niche chemoprotection mediated by cytochrome P450 enzymes.
714 *Oncotarget* 6:14905-14912.
715 Arai, F., A. Hirao, M. Ohmura, H. Sato, S. Matsuoka, K. Takubo, K. Ito, G.Y. Koh, and T. Suda.
716 2004. Tie2/angiopoietin-1 signaling regulates hematopoietic stem cell quiescence
717 in the bone marrow niche. *Cell* 118:149-161.
718 Armulik, A., G. Genove, and C. Betsholtz. 2011. Pericytes: developmental, physiological,
719 and pathological perspectives, problems, and promises. *Developmental cell*
720 21:193-215.
721 Bakst, R.L., M.S. Tallman, D. Douer, and J. Yahalom. 2011. How I treat extramedullary acute
722 myeloid leukemia. *Blood* 118:3785-3793.
723 Baryawno, N., D. Przybylski, M.S. Kowalczyk, Y. Kfoury, N. Severe, K. Gustafsson, K.D.
724 Kokkaliaris, F. Mercier, M. Tabaka, M. Hofree, D. Dionne, A. Papazian, D. Lee, O.
725 Ashenberg, A. Subramanian, E.D. Vaishnav, O. Rozenblatt-Rosen, A. Regev, and D.T.

726 Scadden. 2019. A Cellular Taxonomy of the Bone Marrow Stroma in Homeostasis
727 and Leukemia. *Cell* 177:1915-1932 e1916.
728 Batsivari, A., M.L.R. Haltalli, D. Passaro, C. Pospori, C. Lo Celso, and D. Bonnet. 2020.
729 Dynamic responses of the haematopoietic stem cell niche to diverse stresses. *Nat*
730 *Cell Biol* 22:7-17.
731 Cai, H., M. Kondo, L. Sandhow, P. Xiao, A.S. Johansson, T. Sasaki, J. Zawacka-Pankau, K.
732 Tryggvason, J. Ungerstedt, J. Walfridsson, M. Ekblom, and H. Qian. 2022. Critical
733 role of Lama4 for hematopoiesis regeneration and acute myeloid leukemia
734 progression. *Blood* 139:3040-3057.
735 Calvi, L.M., G.B. Adams, K.W. Weibrecht, J.M. Weber, D.P. Olson, M.C. Knight, R.P. Martin,
736 E. Schipani, P. Divieti, F.R. Bringhurst, L.A. Milner, H.M. Kronenberg, and D.T.
737 Scadden. 2003. Osteoblastic cells regulate the haematopoietic stem cell niche.
738 *Nature* 425:841-846.
739 Dong, L., W.M. Yu, H. Zheng, M.L. Loh, S.T. Bunting, M. Pauly, G. Huang, M. Zhou, H.E.
740 Broxmeyer, D.T. Scadden, and C.K. Qu. 2016. Leukaemogenic effects of Ptpn11
741 activating mutations in the stem cell microenvironment. *Nature* 539:304-308.
742 Duarte, D., E.D. Hawkins, O. Akinduro, H. Ang, K. De Filippo, I.Y. Kong, M. Haltalli, N. Ruivo,
743 L. Straszkowski, S.J. Vervoort, C. McLean, T.S. Weber, R. Khorshed, C. Pirillo, A. Wei,
744 S.K. Ramasamy, A.P. Kusumbe, K. Duffy, R.H. Adams, L.E. Purton, L.M. Carlin, and
745 C. Lo Celso. 2018. Inhibition of Endosteal Vascular Niche Remodeling Rescues
746 Hematopoietic Stem Cell Loss in AML. *Cell Stem Cell* 22:64-77 e66.
747 Farge, T., E. Saland, F. de Toni, N. Aroua, M. Hosseini, R. Perry, C. Bosc, M. Sugita, L. Stuani,
748 M. Fraisse, S. Scotland, C. Larrue, H. Boutzen, V. Feliu, M.L. Nicolau-Travers, S.
749 Cassant-Sourdy, N. Broin, M. David, N. Serhan, A. Sarry, S. Tavitian, T. Kaoma, L.
750 Vallar, J. Iacovoni, L.K. Linares, C. Montersino, R. Castellano, E. Griessinger, Y.
751 Collette, O. Duchamp, Y. Barreira, P. Hirsch, T. Palama, L. Gales, F. Delhommeau,
752 B.H. Garmy-Susini, J.C. Portais, F. Vergez, M. Selak, G. Danet-Desnoyers, M. Carroll,
753 C. Recher, and J.E. Sarry. 2017. Chemotherapy-Resistant Human Acute Myeloid
754 Leukemia Cells Are Not Enriched for Leukemic Stem Cells but Require Oxidative
755 Metabolism. *Cancer discovery* 7:716-735.
756 Forte, D., M. Garcia-Fernandez, A. Sanchez-Aguilera, V. Stavropoulou, C. Fielding, D.
757 Martin-Perez, J.A. Lopez, A.S.H. Costa, L. Tronci, E. Nikitopoulou, M. Barber, P.
758 Gallipoli, L. Marando, C.L. Fernandez de Castillejo, A. Tzankov, S. Dietmann, M.
759 Cavo, L. Catani, A. Curti, J. Vazquez, C. Frezza, B.J. Huntly, J. Schwaller, and S.
760 Mendez-Ferrer. 2020. Bone Marrow Mesenchymal Stem Cells Support Acute
761 Myeloid Leukemia Bioenergetics and Enhance Antioxidant Defense and Escape
762 from Chemotherapy. *Cell Metab*
763 Gouache, E., V. Greze, M. Strullu, P. Saultier, O. Fenneteau, V. Gandemer, C. Ragu, A.
764 Auvrignon, H. Boutroux, H. Lapillonne, M. Pasquet, and G. Leverger. 2018.
765 Leukemia Cutis in Childhood Acute Myeloid Leukemia: Epidemiological, Clinical,
766 Biological, and Prognostic Characteristics of Patients Included in the ELAM02
767 Study. *Hemasphere* 2:e141.
768 Greenbaum, A., Y.M. Hsu, R.B. Day, L.G. Schuettpelz, M.J. Christopher, J.N. Borgerding, T.
769 Nagasawa, and D.C. Link. 2013. CXCL12 in early mesenchymal progenitors is
770 required for haematopoietic stem-cell maintenance. *Nature* 495:227-230.
771 Gu, Y.C., J. Kortesmaa, K. Tryggvason, J. Persson, P. Ekblom, S.E. Jacobsen, and M. Ekblom.
772 2003. Laminin isoform-specific promotion of adhesion and migration of human
773 bone marrow progenitor cells. *Blood* 101:877-885.

774 Han, J., Y.J. Koh, H.R. Moon, H.G. Ryoo, C.H. Cho, I. Kim, and G.Y. Koh. 2010. Adipose tissue
775 is an extramedullary reservoir for functional hematopoietic stem and progenitor
776 cells. *Blood* 115:957-964.
777 Hanoun, M., D. Zhang, T. Mizoguchi, S. Pinho, H. Pierce, Y. Kunisaki, J. Lacombe, S.A.
778 Armstrong, U. Duhrsen, and P.S. Frenette. 2014. Acute myelogenous leukemia-
779 induced sympathetic neuropathy promotes malignancy in an altered
780 hematopoietic stem cell niche. *Cell stem cell* 15:365-375.
781 Hartwell, K.A., P.G. Miller, S. Mukherjee, A.R. Kahn, A.L. Stewart, D.J. Logan, J.M. Negri, M.
782 Duvet, M. Jaras, R. Puram, V. Dancik, F. Al-Shahrour, T. Kindler, Z. Tothova, S.
783 Chattopadhyay, T. Hasaka, R. Narayan, M. Dai, C. Huang, S. Shterental, L.P. Chu, J.E.
784 Haydu, J.H. Shieh, D.P. Steensma, B. Munoz, J.A. Bittker, A.F. Shamji, P.A. Clemons,
785 N.J. Tolliday, A.E. Carpenter, D.G. Gilliland, A.M. Stern, M.A.S. Moore, D.T. Scadden,
786 S.L. Schreiber, B.L. Ebert, and T.R. Golub. 2013. Niche-based screening identifies
787 small-molecule inhibitors of leukemia stem cells. *Nat Chem Biol* 9:840-848.
788 Hoggatt, J., Y. Kfoury, and D.T. Scadden. 2016. Hematopoietic Stem Cell Niche in Health
789 and Disease. *Annual review of pathology* 11:555-581.
790 Hu, Y., and G.K. Smyth. 2009. ELDA: extreme limiting dilution analysis for comparing
791 depleted and enriched populations in stem cell and other assays. *Journal of*
792 *immunological methods* 347:70-78.
793 Iwamoto, S., K. Mihara, J.R. Downing, C.H. Pui, and D. Campana. 2007. Mesenchymal cells
794 regulate the response of acute lymphoblastic leukemia cells to asparaginase. *J Clin*
795 *Invest* 117:1049-1057.
796 Jeong, S.Y., J.A. Kim, and I.H. Oh. 2018. The Adaptive Remodeling of Stem Cell Niche in
797 Stimulated Bone Marrow Counteracts the Leukemic Niche. *Stem Cells*
798 Jin, L., Y. Tabe, S. Konoplev, Y. Xu, C.E. Leysath, H. Lu, S. Kimura, A. Ohsaka, M.B. Rios, L.
799 Calvert, H. Kantarjian, M. Andreeff, and M. Konopleva. 2008. CXCR4 up-regulation
800 by imatinib induces chronic myelogenous leukemia (CML) cell migration to bone
801 marrow stroma and promotes survival of quiescent CML cells. *Mol Cancer Ther*
802 7:48-58.
803 Kim, J.A., J.S. Shim, G.Y. Lee, H.W. Yim, T.M. Kim, M. Kim, S.H. Leem, J.W. Lee, C.K. Min, and
804 I.H. Oh. 2015. Microenvironmental remodeling as a parameter and prognostic
805 factor of heterogeneous leukemogenesis in acute myeloid leukemia. *Cancer Res*
806 Kimlin, L., and V. Virador. 2013. Cellular populations isolated from newborn mouse skin
807 including mesenchymal stem cells. *Methods in molecular biology* 989:217-233.
808 Krooks, J.A., and A.G. Weatherall. 2018. Leukemia cutis in acute myeloid leukemia
809 signifies a poor prognosis. *Cutis* 102:266;271;272.
810 Kusumbe, A.P., S.K. Ramasamy, T. Itkin, M.A. Mae, U.H. Langen, C. Betsholtz, T. Lapidot,
811 and R.H. Adams. 2016. Age-dependent modulation of vascular niches for
812 haematopoietic stem cells. *Nature* 532:380-384.
813 Landberg, N., S. von Palffy, M. Askmyr, H. Lilljebjorn, C. Sanden, M. Rissler, S. Mustjoki, H.
814 Hjorth-Hansen, J. Richter, H. Agerstam, M. Jaras, and T. Fioretos. 2018. CD36
815 defines primitive chronic myeloid leukemia cells less responsive to imatinib but
816 vulnerable to antibody-based therapeutic targeting. *Haematologica* 103:447-455.
817 Liao, Y., G.K. Smyth, and W. Shi. 2013. The Subread aligner: fast, accurate and scalable
818 read mapping by seed-and-vote. *Nucleic acids research* 41:e108.
819 Madapura, H.S., N. Nagy, D. Ujvari, T. Kallas, M.C. Krohnke, S. Amu, M. Bjorkholm, L. Stenke,
820 P.K. Mandal, J.S. McMurray, M. Keszei, L.S. Westerberg, H. Cheng, F. Xue, G. Klein, E.
821 Klein, and D. Salamon. 2017. Interferon gamma is a STAT1-dependent direct

822 inducer of BCL6 expression in imatinib-treated chronic myeloid leukemia cells.
823 *Oncogene*
824 Manshouri, T., Z. Estrov, A. Quintas-Cardama, J. Burger, Y. Zhang, A. Livun, L. Knez, D.
825 Harris, C.J. Creighton, H.M. Kantarjian, and S. Verstovsek. 2011. Bone marrow
826 stroma-secreted cytokines protect JAK2(V617F)-mutated cells from the effects of
827 a JAK2 inhibitor. *Cancer Res* 71:3831-3840.
828 Marlein, C.R., L. Zaitseva, R.E. Piddock, S.D. Robinson, D.R. Edwards, M.S. Shafat, Z. Zhou,
829 M. Lawes, K.M. Bowles, and S.A. Rushworth. 2017. NADPH oxidase-2 derived
830 superoxide drives mitochondrial transfer from bone marrow stromal cells to
831 leukemic blasts. *Blood* 130:1649-1660.
832 McGuckin, C.P., N. Forraz, and W.M. Liu. 2003. Diaminofluorene stain detects erythroid
833 differentiation in immature haemopoietic cells treated with EPO, IL-3, SCF,
834 TGFbeta1, MIP-1alpha and IFNgamma. *European journal of haematology* 70:106-
835 114.
836 Morikawa, S., Y. Mabuchi, Y. Kubota, Y. Nagai, K. Niibe, E. Hiratsu, S. Suzuki, C. Miyauchi-
837 Hara, N. Nagoshi, T. Sunabori, S. Shimmura, A. Miyawaki, T. Nakagawa, T. Suda, H.
838 Okano, and Y. Matsuzaki. 2009. Prospective identification, isolation, and systemic
839 transplantation of multipotent mesenchymal stem cells in murine bone marrow. *J*
840 *Exp Med* 206:2483-2496.
841 Mortazavi, A., B.A. Williams, K. McCue, L. Schaeffer, and B. Wold. 2008. Mapping and
842 quantifying mammalian transcriptomes by RNA-Seq. *Nat Methods* 5:621-628.
843 Moschoi, R., V. Imbert, M. Nebout, J. Chiche, D. Mary, T. Prebet, E. Saland, R. Castellano, L.
844 Pouyet, Y. Collette, N. Vey, C. Chabannon, C. Recher, J.E. Sarry, D. Alcor, J.F. Peyron,
845 and E. Griessinger. 2016. Protective mitochondrial transfer from bone marrow
846 stromal cells to acute myeloid leukemic cells during chemotherapy. *Blood*
847 128:253-264.
848 Omatsu, Y., T. Sugiyama, H. Kohara, G. Kondoh, N. Fujii, K. Kohno, and T. Nagasawa. 2010.
849 The essential functions of adipo-osteogenic progenitors as the hematopoietic stem
850 and progenitor cell niche. *Immunity* 33:387-399.
851 Parsi, M., M.S. Go, and A. Ahmed. 2020. Leukemia Cutis. In StatPearls. Treasure Island
852 (FL).
853 Pena-Martinez, P., M. Eriksson, R. Ramakrishnan, M. Chapellier, C. Hogberg, C. Orsmark-
854 Pietras, J. Richter, A. Andersson, T. Fioretos, and M. Jaras. 2018. Interleukin 4
855 induces apoptosis of acute myeloid leukemia cells in a Stat6-dependent manner.
856 *Leukemia* 32:588-596.
857 Pinho, S., J. Lacombe, M. Hanoun, T. Mizoguchi, I. Bruns, Y. Kunisaki, and P.S. Frenette.
858 2013. PDGFRalpha and CD51 mark human Nestin+ sphere-forming mesenchymal
859 stem cells capable of hematopoietic progenitor cell expansion. *J Exp Med*
860 210:1351-1367.
861 Poulos, M.G., P. Guo, N.M. Kofler, S. Pinho, M.C. Gutkin, A. Tikhonova, I. Aifantis, P.S.
862 Frenette, J. Kitajewski, S. Rafii, and J.M. Butler. 2013. Endothelial Jagged-1 is
863 necessary for homeostatic and regenerative hematopoiesis. *Cell reports* 4:1022-
864 1034.
865 Qian, H., A. Badaloni, F. Chiara, J. Stjernberg, N. Polisetti, K. Nihlberg, G.G. Consalez, and M.
866 Sigvardsson. 2013. Molecular characterization of prospectively isolated
867 multipotent mesenchymal progenitors provides new insight into the cellular
868 identity of mesenchymal stem cells in mouse bone marrow. *Mol Cell Biol* 33:661-
869 677.

870 Qian, H., K. Le Blanc, and M. Sigvardsson. 2012. Primary mesenchymal stem and
871 progenitor cells from bone marrow lack expression of CD44 protein. *The Journal*
872 *of biological chemistry* 287:25795-25807.
873 Raaijmakers, M.H., S. Mukherjee, S. Guo, S. Zhang, T. Kobayashi, J.A. Schoonmaker, B.L.
874 Ebert, F. Al-Shahrour, R.P. Hasserjian, E.O. Scadden, Z. Aung, M. Matza, M.
875 Merkenschlager, C. Lin, J.M. Rommens, and D.T. Scadden. 2010. Bone progenitor
876 dysfunction induces myelodysplasia and secondary leukaemia. *Nature* 464:852-
877 857.
878 Schepers, K., E.M. Pietras, D. Reynaud, J. Flach, M. Binnewies, T. Garg, A.J. Wagers, E.C.
879 Hsiao, and E. Passegue. 2013. Myeloproliferative neoplasia remodels the
880 endosteal bone marrow niche into a self-reinforcing leukemic niche. *Cell Stem Cell*
881 13:285-299.
882 Somervaille, T.C., and M.L. Cleary. 2006. Identification and characterization of leukemia
883 stem cells in murine MLL-AF9 acute myeloid leukemia. *Cancer Cell* 10:257-268.
884 Stier, S., Y. Ko, R. Forkert, C. Lutz, T. Neuhaus, E. Grunewald, T. Cheng, D. Dombkowski,
885 L.M. Calvi, S.R. Rittling, and D.T. Scadden. 2005. Osteopontin is a hematopoietic
886 stem cell niche component that negatively regulates stem cell pool size. *J Exp Med*
887 201:1781-1791.
888 Susek, K.H., E. Korpos, J. Huppert, C. Wu, I. Savelyeva, F. Rosenbauer, C. Muller-Tidow, S.
889 Koschmieder, and L. Sorokin. 2018. Bone marrow laminins influence
890 hematopoietic stem and progenitor cell cycling and homing to the bone marrow.
891 *Matrix Biol* 67:47-62.
892 Thoren, L.A., K. Liuba, D. Bryder, J.M. Nygren, C.T. Jensen, H. Qian, J. Antonchuk, and S.E.
893 Jacobsen. 2008. Kit regulates maintenance of quiescent hematopoietic stem cells.
894 *J Immunol* 180:2045-2053.
895 Thyboll, J., J. Kortesmaa, R. Cao, R. Soininen, L. Wang, A. Iivanainen, L. Sorokin, M. Risling,
896 Y. Cao, and K. Tryggvason. 2002. Deletion of the laminin alpha4 chain leads to
897 impaired microvessel maturation. *Mol Cell Biol* 22:1194-1202.
898 Toma, J.G., M. Akhavan, K.J.L. Fernandes, F. Barnabe-Heider, A. Sadikot, D.R. Kaplan, and
899 F.D. Miller. 2001. Isolation of multipotent adult stem cells from the dermis of
900 mammalian skin. *Nat Cell Biol* 3:778-784.
901 Vaculik, C., C. Schuster, W. Bauer, N. Iram, K. Pfisterer, G. Kramer, A. Reinisch, D. Strunk,
902 and A. Elbe-Burger. 2012. Human dermis harbors distinct mesenchymal stromal
903 cell subsets. *J Invest Dermatol* 132:563-574.
904 van Os, R.P., B. Dethmers-Ausema, and G. de Haan. 2008. In vitro assays for cobblestone
905 area-forming cells, LTC-IC, and CFU-C. *Methods Mol Biol* 430:143-157.
906 Viswanathan, S., Y. Shi, J. Galipeau, M. Krampera, K. Leblanc, I. Martin, J. Nolta, D.G.
907 Phinney, and L. Sensebe. 2019. Mesenchymal stem versus stromal cells:
908 International Society for Cell & Gene Therapy (ISCT(R)) Mesenchymal Stromal Cell
909 committee position statement on nomenclature. *Cytotherapy* 21:1019-1024.
910 Wang, C.X., I. Pusic, and M.J. Anadkat. 2019. Association of Leukemia Cutis With Survival
911 in Acute Myeloid Leukemia. *JAMA Dermatol* 155:826-832.
912 Welner, R.S., G. Amabile, D. Bararia, A. Czibere, H. Yang, H. Zhang, L.L. Pontes, M. Ye, E.
913 Levantini, A. Di Ruscio, G. Martinelli, and D.G. Tenen. 2015. Treatment of chronic
914 myelogenous leukemia by blocking cytokine alterations found in normal stem and
915 progenitor cells. *Cancer Cell* 27:671-681.
916 Xiao, P., M. Dolinska, L. Sandhow, M. Kondo, A.S. Johansson, T. Bouderlique, Y. Zhao, X. Li,
917 M. Dimitriou, G.Z. Rassidakis, E. Hellstrom-Lindberg, N. Minato, J. Walfridsson, D.T.
918 Scadden, M. Sigvardsson, and H. Qian. 2018a. Sipa1 deficiency-induced bone

919 marrow niche alterations lead to the initiation of myeloproliferative neoplasm.
920 *Blood advances* 2:534-548.
921 Xiao, P., L. Sandhow, Y. Heshmati, M. Kondo, T. Bouderlique, M. Dolinska, A.S. Johansson,
922 M. Sigvardsson, M. Ekblom, J. Walfridsson, and H. Qian. 2018b. Distinct roles of
923 mesenchymal stem and progenitor cells during the development of acute myeloid
924 leukemia in mice. *Blood advances* 2:1480-1494.
925 Xu, X., X. Zhang, Y. Liu, L. Yang, S. Huang, L. Lu, S. Wang, Q. Guo, and L. Zhao. 2016. BM
926 microenvironmental protection of CML cells from imatinib through Stat5/NF-
927 kappaB signaling and reversal by Wogonin. *Oncotarget* 7:24436-24454.
928 Ye, H., B. Adane, N. Khan, T. Sullivan, M. Minhajuddin, M. Gasparetto, B. Stevens, S. Pei, M.
929 Balys, J.M. Ashton, D.J. Klemm, C.M. Woolthuis, A.W. Stranahan, C.Y. Park, and C.T.
930 Jordan. 2016. Leukemic Stem Cells Evade Chemotherapy by Metabolic Adaptation
931 to an Adipose Tissue Niche. *Cell Stem Cell* 19:23-37.
932 Zhang, B., M. Li, T. McDonald, T.L. Holyoake, R.T. Moon, D. Campana, L. Shultz, and R.
933 Bhatia. 2013. Microenvironmental protection of CML stem and progenitor cells
934 from tyrosine kinase inhibitors through N-cadherin and Wnt-beta-catenin
935 signaling. *Blood* 121:1824-1838.
936
937

938 **Figure Legends**

939

940 **Figure 1 AML cells infiltrated in skin are capable to regenerate AML post-**
941 **transplantation**

942 (**A**) Strategy to generate MLL-AF9 AML mouse model. MLL-AF9 transduced AML cells
943 expressing CD45.1 were transplanted into non-irradiated CD45.2 C57BL/6 mice.
944 (**B**) FACS profile showing AML engraftment analysis in BM, peripheral blood (PB), spleen
945 and dorsal skin at the end stage of AML. The numbers in the panel are the mean frequencies.
946 (**C**) Proportion of the AML cells within total hematopoietic ($CD45^+$) cell in blood, skin, BM
947 and spleen. Data were from 2 independent experiments and each dot represents data from one
948 mouse. The horizontal bars represent mean values. n=4-9 per group, * $P<0.05$, ** $P<0.01$, ****
949 $P<0.0001$, determined by paired *t*-test except the comparison between skin and blood where
950 unequal number of the mice were included.
951 **(D)** The inverse correlation between AML engraftment in the skin with symptomatic AML
952 onset. * $P<0.05$, determined by Spearman correlation. Each dot represents data from a single
953 recipient mouse, n=18 mice.
954 (**E**) Confocal image showing distribution of MLL-$AF9^+$ AML cells expressing DsRed at
955 perivascular sites in dorsal skin. The AML cells were injected after sublethal irradiation of the
956 mice. The endothelial cells were marked by CD31 expression (white). Scale bars are 50 μm.

957 (**F**) Experimental strategy to assess AML-initiating capacity of the AML cells infiltrated in
958 mouse skin by serial transplantation. The primary recipient mice (CD45.2) that developed
959 AML post-AML cell (CD45.1) transplantation were treated with Ara-C (100mg/Kg) or saline
960 (NS, untreated) for 5 days. The residual CD45.1$^+$ AML cells from skin were sorted at 2-3 days
961 after the last injection of Ara-C and transplanted into secondary non-irradiated recipient
962 CD45.2 mice at doses of 10, 100, 1000 (1K) and 5000 (5K) cells/mouse. The AML
963 development was monitored by FACS and hematology analyzer Sysmex. The mice were
964 sacrificed when found moribund.
965 (**G**) AML engraftment in blood, skin, BM and spleen of the primary recipients under steady
966 state and 3 days post-Ara-C treatment. Each dot represents data from a single mouse. n=5 per
967 group, * P<0.05, **** P<0.0001, determined by paired *t*-test
968 (**H**) The fraction of CD36$^+$ AML cells in the skin, BM and spleen. Each dot represents data
969 from a single mouse. ns, no significant difference, determined by paired *t*-test.
970 (**I**) The frequency of CFU-Cs derived from the residual AML cells in skin, spleen and BM.
971 (**J**) The Kaplan-Meier survival curve of the primary and secondary recipient mice. The curve
972 was generated by Log-rank (Mantel-Cox test). Each dot represents an endpoint when the mice
973 were found dead or sacrificed because of being moribund. Data were from 2 independent
974 experiments. n=5-8 primary recipients treated with Ara-C (n=5) or normal saline (untreated),
975 n=5-7 secondary recipients per group.
976 (**K**) Platelet counts in PB of the secondary recipient mice at the endpoint. Each dot represents
977 data from a single mouse.
978 (**L**) Spleen size of the secondary recipient mice at the endpoint. Each dot represents data from
979 a single mouse.
980 (**M**) FACS profile showing the engraftment of skin-derived AML CD45.1$^+$ cells in BM of the
981 secondary recipient mice.
982 (**N**) AML engraftment of the skin-derived AML CD45.1$^+$ cells in BM of the secondary
983 recipient mice. Each dot represents data from a single mouse.
984 (**O**) The frequencies of the secondary recipient mice that developed AML after injection of
985 skin-derived AML cells. The frequency of AML-initiating LSCs was determined by Extreme
986 Limiting Dilution analysis (Hu and Smyth, 2009) based on the number of mice that developed
987 AML post-secondary transplantation. ns, no significant difference, determined by *Chi* square
988 test.
989 (**P**) The % of AML-initiating LSCs in BM and skin. The percentages were calculated based on
990 the frequencies of AML-initiating LSCs determined by transplantation and shown in (G) and

991 the % AML cells within total $CD45^+$ mononuclear cells in each tissue. Each dot represents data
992 from a single mouse. n=5-8 per group, ns, no significant difference, **** P<0.0001,
993 determined by unpaired *t*-test.
994 See also in Figure S1.
995
996 **Figure 2 Identification of skin MPC subsets by Ebf2 expression.**
997 (**A**) A representative FACS profile showing FACS sorting/analysis of the $Ebf2^+$ and $Ebf2^-$ cells
998 in dorsal skin. The cells were first gated within non-hematopoietic ($CD45^-TER119^-$) and non-
999 endothelial ($CD31^-$) live (PI^-) stromal cells. These cells lacking expression of CD44 were
1000 further analyzed for their expression of SCA1, PDGFRa/CD140a (PαS) and CD51. The
1001 numbers in the panel are the mean frequencies.
1002 (**B-C**) The $Ebf2^+$ cell frequency within total PI^- (**B**) or $PI^-CD45^-TER119^-CD31^-$ stromal cells
1003 (**C**) in dorsal skin.
1004 (**D**) The fractions of PαS cells within the $Ebf2^+$ and $Ebf2^-$ stromal cells. Each dot in **B-D**
1005 represents data from a single mouse in 3-6 experiments with the horizontal line as a mean value.
1006 (**E**) CFU-Fs in the $Ebf2^+$ and $Ebf2^-$ stromal cells.
1007 (**F**) CFU-Fs were exclusively found in the $Ebf2^+SCA1^+$ cell fraction. Data in **E-F** are from 3
1008 independent experiments and each dot represents replicate assays from 2-3 mice in each
1009 experiment. The horizontal line represents mean value. *** P<0.001, **** P<0.0001,
1010 determined by Wilcoxon matched-signed pair rank test.
1011 **(G-J)** Single-cell analysis of CFU-Fs and lineage differentiation from the FACS-sorted $Ebf2^+$
1012 (**G-H**) and $Ebf2^-$PαS (**I-J**) stromal cells. The CFU-F frequencies (**G**, **I**) were determined by
1013 limiting dilution at a density of 1, 2, 5, 10 cells per well in a 96-well plate and the frequency
1014 of the single cells with bi-lineage plasticity (**H, J**) were assessed by multilineage differentiation
1015 potential of single CFU-Fs derived from the cells. The simple linear regression was used to
1016 determine the dose responses in G and I.
1017 (**K**) Representative images of the osteogenic and adipogenic differentiation from single CFU-
1018 F clones derived from $Ebf2^+$ and $Ebf2^-$PαS cells. Scale bars in the images for $Ebf2^+$ cells are
1019 100 μm, and 250 μm and 100 μm in the images for osteogenic and adipogenic differentiation
1020 from $Ebf2^-$PαS cells.
1021 (**L**) Population-doubling time (PDT) of randomly selected CFU-Fs derived from single $Ebf2^+$
1022 and $Ebf2^-$PαS cells. Each line represents the growth kinetics of a single clone.
1023 See also in Figure S2.

1024

1025 **Figure 3 Distribution and hierarchical relationship of skin MPCs.**

1026 (**A**) Localization of Ebf2$^+$ cells in skin perivascular area and in dermal panniculus carnosus
1027 (DPC). The endothelial cells in the vessels were identified by MECA32 staining. Arrows point
1028 to the Ebf2$^+$ cells in DPC area. Scale bars are 100 μm.

1029 (**B**) Representative image showing the perivascular localization of Ebf2$^+$ cells adjacent to
1030 CD31$^+$ endothelial cells in dorsal skin. Scale bars are 10 μm.

1031 (**C**) A scheme showing strategy for lineage-tracing of the Ebf2$^+$ cells in skin. The
1032 Ebf2/GFP$^+$Tomato$^+$ cells and their progenies (Ebf2/GFP$^-$Tomato$^+$) were traced by FACS at 3,
1033 6, 12 months after tamoxifen injection.

1034 (**D**) A representative FACS profile showing analysis of activated Ebf2$^+$ cells (GFP$^+$Tomato$^+$)
1035 and their progeny (GFP$^-$Tomato$^+$). The gates for different cell subsets were defined with FMO
1036 from bi-transgenic or single transgenic mice. Each stromal cell subset (PI$^-$CD45$^-$TER119$^-$
1037 CD31$^-$) was gated within the CD44$^-$ fractions and subsequently gated for PαS cells based on
1038 CD140a and SCA1 expression.

1039 (**E**) The frequencies of Ebf2/GFP$^+$Tomato$^+$ cells and its progenies (Ebf2/GFP$^-$Tomato$^+$) within
1040 stromal cells. Each dot represents data from each mouse from 2-3 independent experiments.
1041 Horizontal bars represent the mean, * $P<0.05$, determined by unpaired *t*-test.

1042 (**F**) The fractions of PαS and Ebf2$^-$CD140a$^+$SCA1$^-$ cells within total GFP$^-$Tomato$^+$ cells
1043 generated by Ebf2$^+$ cells. Each dot represents data from each mouse from 2-3 independent
1044 experiments. Horizontal bars represent the mean, *** $P<0.001$, determined by unpaired *t*-test.

1045 (**G**) Distribution of the single Ebf2/GFP$^+$Tomato$^-$ cells (green), activated Ebf2/GFP$^+$Tomato$^+$
1046 cells (orange) and Ebf2/GFP$^-$Tomato$^+$ (red) cells at 3 months after tamoxifen injection. Scale
1047 bars are 20 μm.

1048 See also in Figure S3-S4.

1049

1050 **Figure 4 Skin MPCs support AML LSC growth and protect them from chemotherapy.**

1051 (**A**) Experimental strategy for assessing the role of the skin MPC and BM MSC subsets for
1052 AML growth by cobblestone area-forming cell (CAFC) assay.

1053 (**B**) Representative images of CAFCs derived from the AML cells. Scale bars are 100 μm.

1054 (**C**) Total numbers of CAFCs generated from 150 MLL-AF9$^+$ AML cells.

1055 (**D**) A proportion of residual CAFCs from AML cells after Ara-C treatment relative to the
1056 normal saline (NS)-treated controls.

1057 (**E**) The total number of the AML cells at 10 days after Ara-C treatment.
1058 (**F-G**) The frequency (F) and the numbers (G) of the KIT^+ AML LSCs.
1059 (**H-I**) The frequency (H) and the numbers (I) of the $CD36^+$ chemoresistant AML cells.
1060 Data in C-I were from 3-4 independent experiments and each dot represents the mean of
1061 replicate assays. The horizontal bars represent mean values. * P<0.05, ** P<0.01, *** P<0.001,
1062 determined by unpaired (C-D, G, I) or paired (E-F,H) *t*-test between Ara-C treated and
1063 nontreated co-cultures within the same stromal cell type. # P<0.05, ## P<0.01, ### P<0.001
1064 determined by unpaired t test when comparing the Ara-C treated AML cells in co-cultures with
1065 BM MSCs or skin MPCs with the Ara-C treated AML monoculture.
1066 (**J**) Co-localization of AML cells (red) with the $Ebf2^+$ cells. Ebf2 was determined by GFP
1067 (green) and the endothelial cells were marked by CD31 (white). Scale bars are 20 μm.
1068 (**K**) Representative FACS plot showing analysis of $Ebf2^+$ MPCs in AML mouse dorsal skin.
1069 (**L**) The frequency of the $Ebf2^+$ MPCs within stromal cells in dorsal skin tissue at endstage of
1070 AML. Data were from 6 independent experiments and each dot represents data from one mouse.
1071 The horizontal bars represent mean values. ** P<0.01, determined by unpaired *t*-test.
1072 (**M**) Representative FACS plot showing analysis of the skin $Ebf2^-$PαS MPCs in healthy
1073 controls and AML mice.
1074 (**N**) The frequency of the $Ebf2^-$PαS cells within stromal cells in dorsal skin at the end stage of
1075 AML. Data were from 6 independent experiments and each dot represents a mouse. The
1076 horizontal bars represent mean values. ns, no significant difference, determined by unpaired *t*-
1077 test.
1078 (**O**) FACS profile showing analysis of $CD31^+$ cells in the dorsal skin of healthy and AML mice.
1079 (**P**) The frequency of total endothelial cells ($CD31^+$) and arteriolar endothelial cells
1080 ($CD31^+SCA1^+$). ns, no significant difference, * P<0.05, determined by Mann-Whitney test.
1081
1082 **Figure 5 RNA sequencing revealed the molecular profile of skin $Ebf2^+$ and $Ebf2^-$PαS**
1083 **MPCs.**
1084 (**A**) Venn diagram showing differentially expressed genes (DEG) among the skin $Ebf2^+$ MPCs,
1085 skin $Ebf2^-$PαS MPCs and BM MSCs.
1086 (**B**) Gene set enrichment analysis (GSEA) revealed the enrichment of genes associated with
1087 different biological processes and cellular responses in the skin $Ebf2^+$ and $Ebf2^-$PαS MPC
1088 subsets.

1089 (**C**) A volcano plot showing differentially expressed genes between skin MPCs (Ebf2$^+$ and
1090 Ebf2$^-$PαS) and BM MSCs.
1091 (**D**) GSEA revealed the enrichment of gene sets associated with various biological processes
1092 and cellular responses in the skin MPCs (Ebf2$^+$ and Ebf2$^-$PαS) and BM MSCs.
1093 (**E**) GSEA plots showing the enrichment of genes related to oxidative phosphorylation,
1094 inflammatory, interferon alpha response and chondrocyte differentiation in the skin MPCs
1095 compared to that in BM MSCs. FDR (false discovery rate). * P<0.05, *** P<0.001, determined
1096 by GSEA software.
1097 (**F**) Heatmap showing the expressions of selected inflammatory cytokines in skin Ebf2$^+$ cells,
1098 Ebf2$^-$PαS cells and BM MSCs. The heatmap was created in Excel using conditional formatting.
1099 The color scale was set based on the minimum, midpoint and maximum values of each gene in
1100 each row. Red correlates with high expression and green correlates with low expression.
1101 (**G**) Gene set enrichment plot showing hematopoiesis supportive niche genes in skin MPC
1102 subsets and BM MSCs, and the heatmap showing the gene expression levels. ns, no significant
1103 difference, determined by GSEA software.
1104 (**H**) Q-PCR of HSC niche genes in BM MSCs, skin Ebf2$^+$ and Ebf2$^-$PαS MPCs. Each dot
1105 represents mean of triplicate measurement of the gene expression relative to *Hprt*. Horizontal
1106 bars represent the mean values. Data were from 3 independent sorting experiments. ns, no
1107 significant difference, * P<0.05, ** P<0.01, determined by unpaired *t*-test.
1108
1109 **Figure 6 Mitochondrial transfer and Lama4 deficiency in skin MPCs contributed to the**
1110 **chemoprotection of AML cells from Ara-C.**
1111 (**A-B**) Increased mitochondrial mass in skin MPCs compared to that in BM MSCs. (A) Mean
1112 fluorescence intensity (MFI) of MitoTracker red in BM MSCs and skin PαS MPCs. Each dot
1113 represents an individual assay in triplicate from 3 independent experiments. * P<0.05,
1114 determined by paired *t*-test. (B) Representative FACS histograms showing MitoTracker red
1115 staining in the skin MPCs and BM MSCs.
1116 (**C**) Experimental strategy for determining mitochondrial transfer from stromal cells to AML
1117 cells *in vitro*. Skin MPCs and BM MSCs that were pre-labelled with MitoTracker red were co-
1118 cultured with MLL-AF9$^+$ AML cells for 24 hours. Ara-C was added 4-6 hours after seeding
1119 the AML cells. The stromal cell-derived mitochondria were detected by MFI of MitoTracker
1120 in the AML cells at 24h post-co-culture by FACS.

1121 (**D**) MFI of MitoTracker showing increased mitochondrial transfer from skin MPCs to AML
1122 cells than that from BM MSCs in the cocultures. Data shown are normalized MitoTracker MFI
1123 in the AML cells based on the values of that in the AML cells co-cultured with BM MSCs
1124 without Ara-C treatment. Each dot represents mean values of 3-4 replicated measurements in
1125 each experiment of 4. Horizontal bars are median values. * P<0.05, ** P<0.01, *** P<0.001,
1126 determined by Kolmogorov-Smirnov test.
1127 (**E**) Representative FACS histograms showing MitoTracker staining in the AML cells 24h post-
1128 co-culture with the stromal cells. The MFI from AML cells in the monoculture without the
1129 prelabeled MPCs was used as a negative control.
1130 (**F**) Reduced ROS levels in the AML cells co-cultured with skin PαS MPCs compared to that
1131 with BM MSCs 24h post-Ara-C treatment. Each dot represents the average value of triplicate
1132 assays from each experiment of 3. Horizontal bars are mean values. * P<0.05, determined by
1133 paired *t*-test.
1134 (**G**) The % of PI^- live AML cells in the cocultures 24h after Ara-C treatment. Each dot
1135 represents mean values of 3-4 replicated measurements in each experiment of 4. Horizontal
1136 bars are median values. The statistical differences were determined by unpaired *t*-test, ns, no
1137 significant difference, ** P<0.01, *** P<0.001, **** P<0.0001.
1138 (**H-J**) Impaired protective mitochondrial transfer from skin MPCs to AML cells in the
1139 cocultures after treatment with microtubule inhibitors. (**H**) MFIs of MitoTracker green in AML
1140 cells co-cultured with skin MPCs and treated with colchicine, nocodazole alone or in
1141 combination with Ara-C. The MFIs were normalized to the nontreated controls, from 4
1142 independent experiments. Each dot represents a single measurement. *P<0.05, ** P<0.01,
1143 determined by unpaired *t*-test. (**I**) Representative histogram showing fluorescence intensity of
1144 mitotracker green in the AML cells. (**J**) The numbers of live AML cells co-cultured with skin
1145 MPCs after the treatments. ** P<0.01, determined by unpaired *t*-test.
1146 (**K-L**) Little mitochondrial transfer from skin or BM MSCs to normal BM HSPCs 24h post-
1147 coculture. The purified $LIN^-SCA1^+KIT^+$ (LSK) cells were co-cultured with MitoTracker green
1148 prelabelled skin MPCs for 24h. The MitoTracker $green^+$ LSK cells were analyzed post-co-
1149 culture based on CD45 expression, as shown in the FACS profile (K) and (L) the % of
1150 MitoTracker $green^+$ LSK cells in co-cultures and monoculture. Each dot represents a replicate
1151 measurement.
1152 (**M**) Experimental layout for assessing the impact of *Lama4* loss in skin MPCs for AML growth
1153 *in vitro* using a co-culture system. The $Lama4^{+/+}$ and $Lama4^{-/-}$ skin MPCs were co-cultured
1154 with MLL-AF9 AML cells in a 96-well plate. For CAFC assay, Ara-C was added 2 days post-

1155 seeding of AML cells. The numbers of total AML cells and CAFCs were counted at 24-28h
1156 and day 7 post-seeding AML cells, respectively.
1157 (**N**) Fold changes in the number of the AML cells in the co-cultures with *Lama4*$^{-/-}$ skin MPCs
1158 in relation to that with *Lama4*$^{+/+}$ MPCs 24hours after Ara-C or NS treatment. Data were from
1159 4 independent experiments and each dot represents the mean of triplicate assays. The horizontal
1160 bars represent mean values. *P<0.05, ** P<0.01, determined by paired *t*-test.
1161 (**O**) The number of CAFCs derived from AML cells in the co-cultures with *Lama4*$^{+/+}$ and
1162 *Lama4*$^{-/-}$ skin MPCs treated with NS or Ara-C. Data shown are triplicate values from 2-3
1163 independent experiments. The horizontal bars represent mean values. *P<0.05, ** P<0.01,
1164 determined by unpaired *t*-test.
1165
1166 **Figure 7 A high level of residual AML cell infiltration in skin tissue of AML-promoting**
1167 ***Lama4*$^{-/-}$ mouse model post Ara-C treatment**.
1168 (**A**) Experimental setup. *Lama4*$^{+/+}$ and *Lama4*$^{-/-}$ mice were first injected with DsRed-expressing
1169 MLL-AF9 AML cells after sublethal irradiation and treated with normal saline (NS) or Ara-C
1170 at day 15 after injection. Peripheral blood (PB) and BM were collected for FACS and confocal
1171 microscopy at 1-day after NS or Ara-C treatment.
1172 (**B**) Representative confocal images showing residual AML cells in dorsal skin at 1-day post-
1173 Ara-C treatment. Scale bars are 500 μm in the panoramic images and 50 μm in the region of
1174 interest (ROI) images.
1175 (**C**) Frequency of AML cells in PB and skin at 1-day post-Ara-C treatment.
1176 (**D**) Proportion of CD36^{+} and KIT^{+} AML LSCs in skin at 1-day post-Ara-C treatment.
1177 Data were from 2-5 experiments and each dot in C-D represents data from a single mouse. The
1178 horizontal bars represent the mean values. n=5-6 per group. ** P<0.01, *** P<0.001,
1179 determined by unpaired *t*-test.
1180 (**E**) Experimental layout for assessing homing of the AML cells into *Lama4*$^{+/+}$ and *Lama4*$^{-/-}$
1181 mice 3 hours after transplantation. CD45.1^{+} MLL-AF9^{+} AML cells (10 million per mouse)
1182 were transplanted into the mice via tail vein injection without prior irradiation. Dorsal skin,
1183 bones, blood of the recipient mice were harvested 3 hours after AML cell transplantation and
1184 the homing of the CD45.1^{+} AML cells was examined by FACS based on CD45.1 expression.
1185 (**F**) Representative FACS profiles showing the gatings of CD45.1^{+} AML cells and CD45.2^{+}
1186 host cells. The gate for CD45.1^{+} cells was determined based on the FMO control without
1187 CD45.1 staining.

1188 (**G**) The frequencies of the AML cells in total live cells in the recipient skin and blood. ns, no
1189 significant difference, determined by unpaired *t*-test. The horizontal bars represent mean values.
1190 Each dot represents individual recipient mouse, n=3-4 per group.
1191 (**H**) The frequencies of the AML cells of total live cells in the *Lama4*$^{+/+}$ and *Lama4*$^{-/-}$ recipient
1192 skin and BM. ns, no significant difference, determined by unpaired *t*-test. The horizontal bars
1193 represent mean values. Each dot represents individual recipient mouse.
1194
1195 **Figure 8 Serial transplantation indicated more residual AML-initiating LSCs in the**
1196 ***Lama4*$^{-/-}$ mouse skin post-Ara-C treatment.**
1197 (**A**) Experimental setup for determining the residual AML-initiating LSCs in the skin of
1198 *Lama4*$^{+/+}$ and *Lama4*$^{-/-}$ mice. The mice were injected with MLL-AF9 AML cells and treated
1199 with normal saline (NS) or Ara-C at day 20 after AML cell injection. The CD45.1^{+} AML cells
1200 were sorted from the skin at 3 days post-Ara-C treatment and intravenously transplanted in
1201 limiting cell doses (10, 100, 1000 cells/mouse) into secondary recipients without prior
1202 irradiation. The AML onset was monitored by FACS of AML cells in blood, spleen and BM.
1203 (**B**) The Kaplan-Meier survival curve of the secondary recipient mice which received skin-
1204 derived AML cells sorted from primary recipients after treatment with Ara-C. The dates were
1205 the days when the mice were found dead or moribund. The survival curve was generated by
1206 Log-rank (Mantel-Cox test). n=5-8 per group.
1207 (**C**) The frequencies of AML-initiating LSCs in the *Lama4*$^{+/+}$ and *Lama4*$^{-/-}$ mouse skin post-
1208 Ara-C treatment. The frequency was determined by Extreme Limiting dilution analysis based
1209 on the frequencies of the secondary mice that developed AML (Hu and Smyth, 2009). ns, no
1210 significant difference, determined by *Chi square* test.
1211 (**D**) The % of total AML cells in the skin of the donor *Lama4*$^{+/+}$ and *Lama4*$^{-/-}$ mice. Each dot
1212 represents data from a single mouse. The horizontal bars represent the median values.
1213 (**E**) The % of AML-initiating LSCs (left) and CFU-Cs (right) within total CD45^{+} cells in the
1214 skin. The data were calculated based on % of AML cells in skin and the frequency (**C**) of the
1215 LSCs and CFU-Cs, respectively. Each dot represents data from a single primary recipient
1216 mouse. The horizontal bars represent the mean values. * $P<0.05$, determined by unpaired *t*-test.
1217 Data were from 2 transplantation experiments.

Figure 1

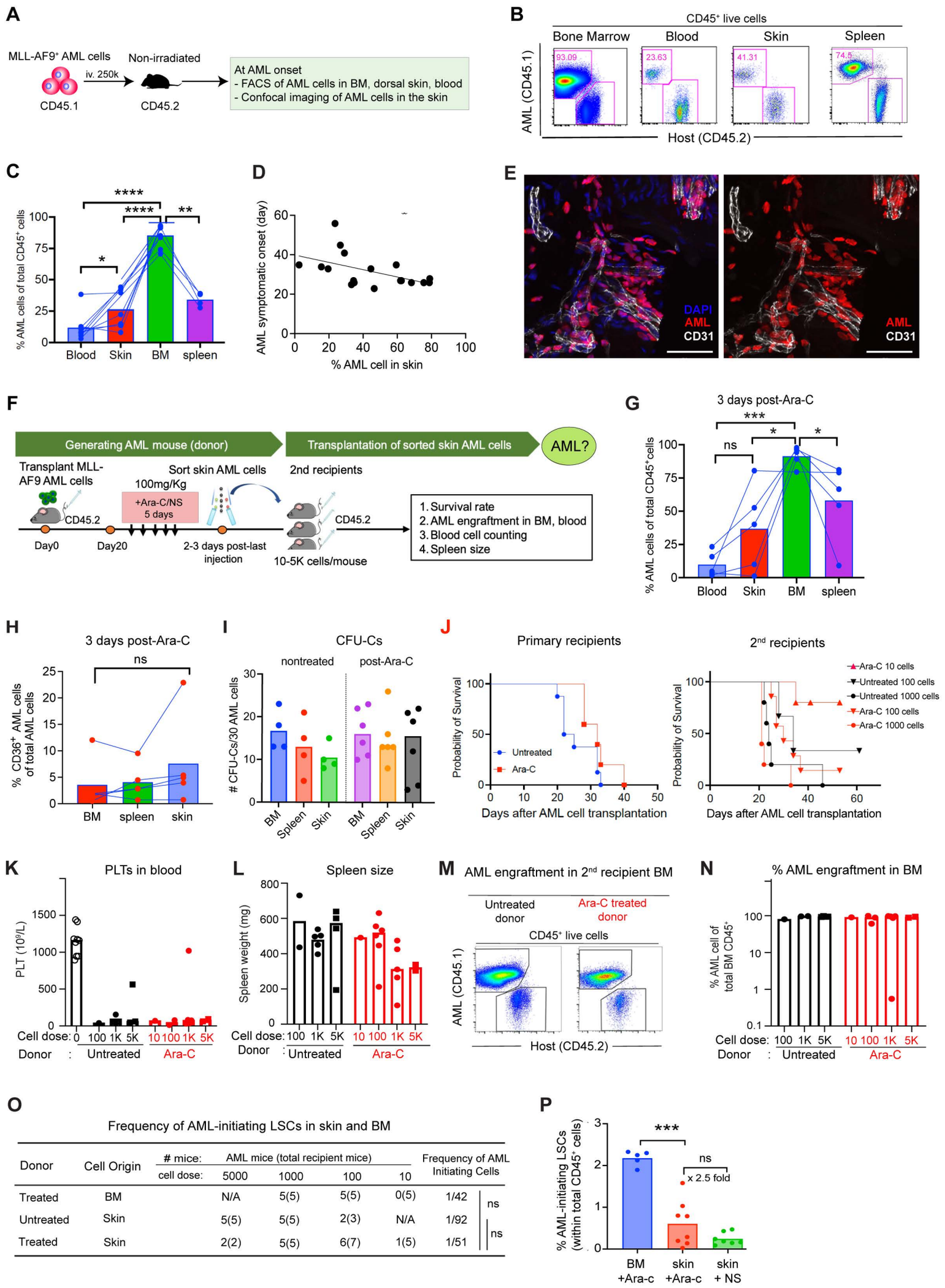

Donor	Cell Origin	# mice: / cell dose:	AML mice (total recipient mice) 5000	1000	100	10	Frequency of AML Initiating Cells	
Treated	BM		N/A	5(5)	5(5)	0(5)	1/42	ns
Untreated	Skin		5(5)	5(5)	2(3)	N/A	1/92	ns
Treated	Skin		2(2)	5(5)	6(7)	1(5)	1/51	

Figure 2

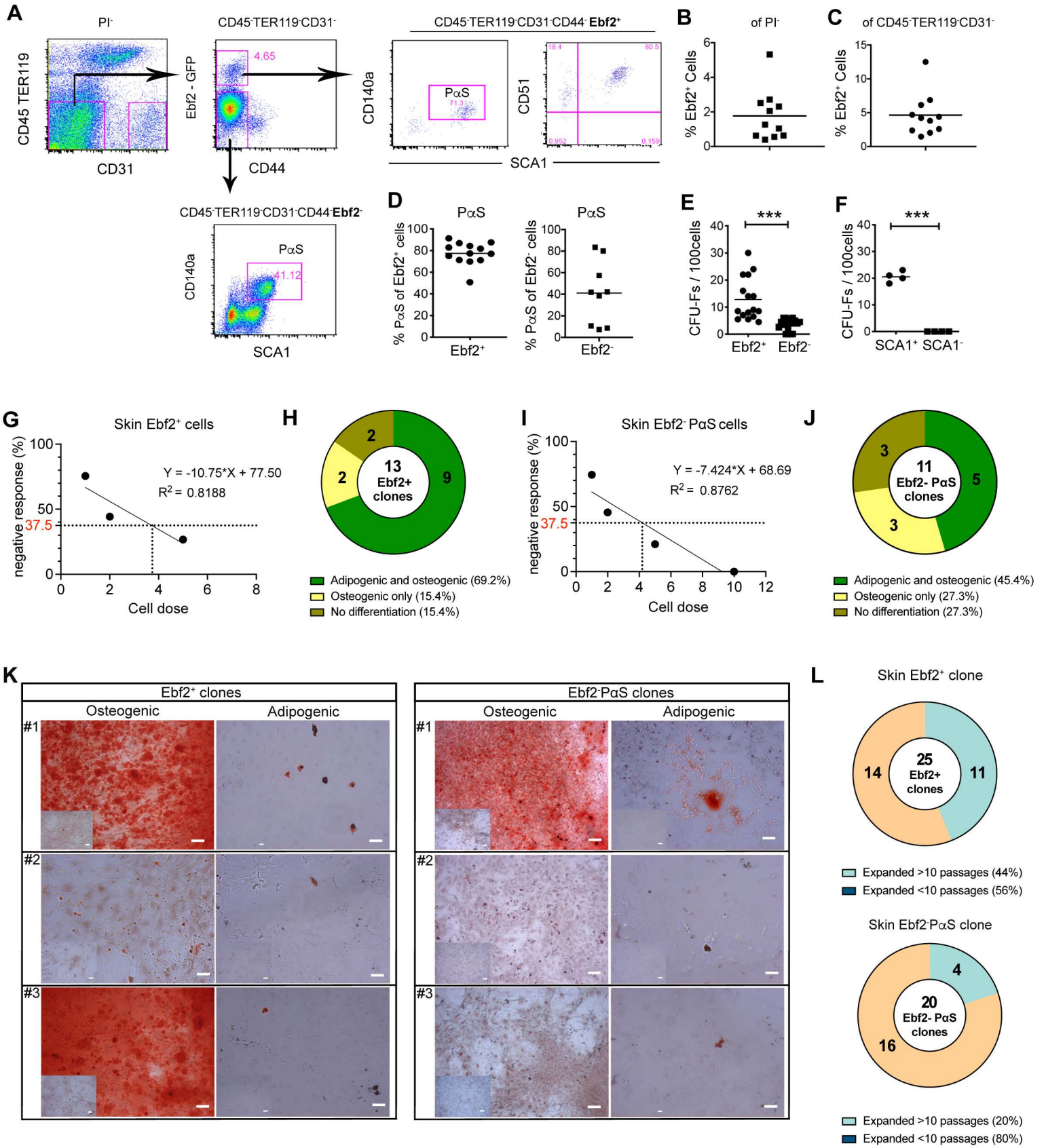
A
PI-
CD45 TER119
CD31
CD45-TER119-CD31-
Ebf2 - GFP
4.65
CD44
CD45-TER119-CD31-CD44-Ebf2+
CD140a
PαS
71.3
CD51
18.4
80.5
0.952
0.159
SCA1
CD45-TER119-CD31-CD44-Ebf2-
CD140a
PαS
41.12
SCA1
B
of PI-
% Ebf2+ Cells
C
of CD45-TER119-CD31-
% Ebf2+ Cells
D
PαS
% PαS of Ebf2+ cells
Ebf2+
PαS
% PαS of Ebf2- cells
Ebf2-
E
***
CFU-Fs / 100cells
Ebf2+
Ebf2-
F
***
CFU-Fs / 100cells
SCA1+
SCA1-
G
Skin Ebf2+ cells
negative response (%)
Y = -10.75*X + 77.50
R2 = 0.8188
37.5
Cell dose
H
13
Ebf2+
clones
9
2
2
Adipogenic and osteogenic (69.2%)
Osteogenic only (15.4%)
No differentiation (15.4%)
I
Skin Ebf2- PαS cells
negative response (%)
Y = -7.424*X + 68.69
R2 = 0.8762
37.5
Cell dose
J
11
Ebf2- PαS
clones
5
3
3
Adipogenic and osteogenic (45.4%)
Osteogenic only (27.3%)
No differentiation (27.3%)
K
Ebf2+ clones
Osteogenic
Adipogenic
#1
#2
#3
Ebf2-PαS clones
Osteogenic
Adipogenic
#1
#2
#3
L
Skin Ebf2+ clone
25
Ebf2+
clones
14
11
Expanded >10 passages (44%)
Expanded <10 passages (56%)
Skin Ebf2-PαS clone
20
Ebf2- PαS
clones
4
16
Expanded >10 passages (20%)
Expanded <10 passages (80%)

Figure 3

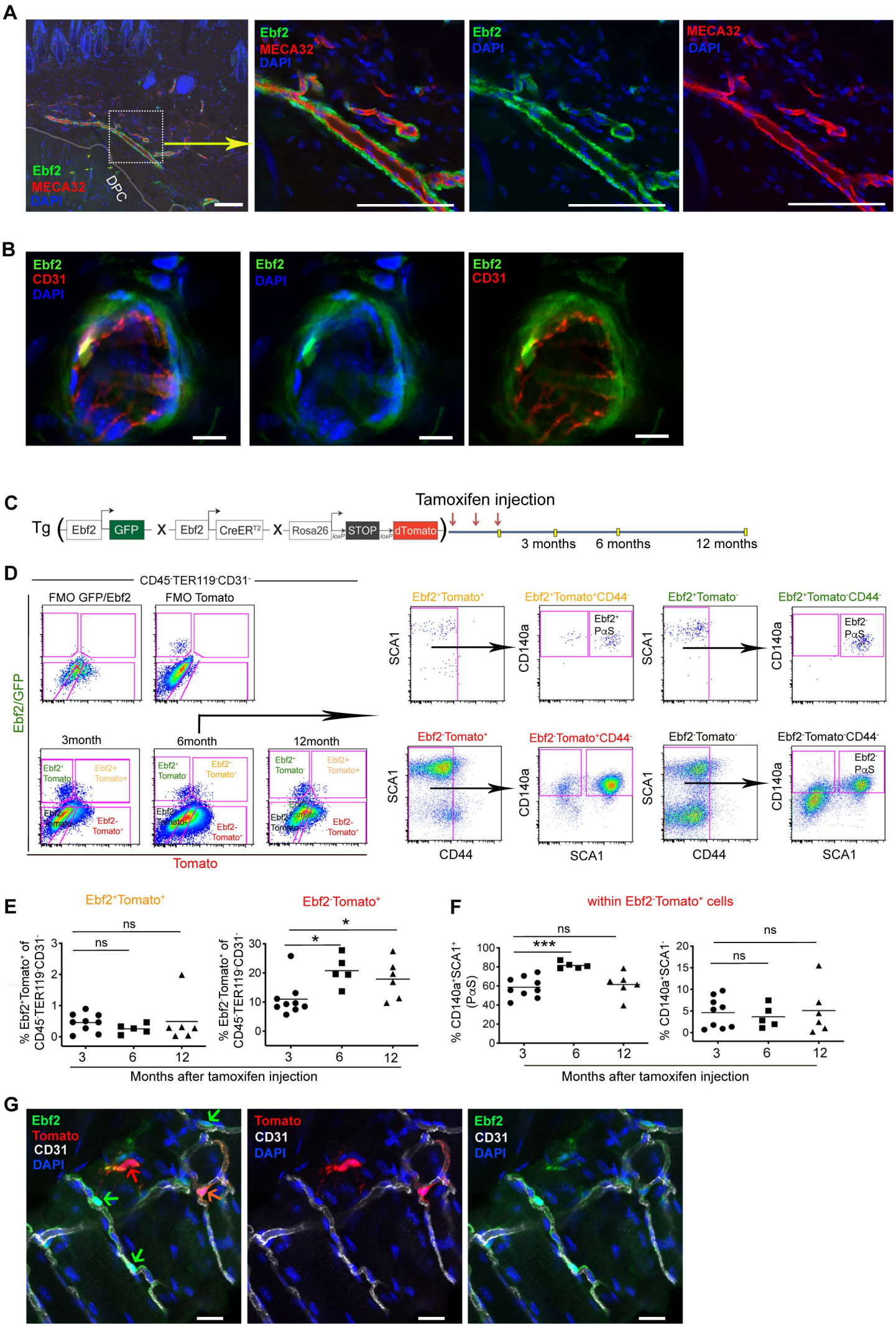
A
Ebf2
MECA32
DAPI
DPC
B
Ebf2
CD31
DAPI
C
Tg
Ebf2
GFP
X
CreER^{T2}
Rosa26
STOP
dTomato
Tamoxifen injection
3 months
6 months
12 months
D
CD45$^-$TER119$^-$CD31$^-$
FMO GFP/Ebf2
FMO Tomato
Ebf2/GFP
3month
6month
12month
Ebf2$^+$Tomato$^-$
Ebf2$^+$Tomato$^+$
Ebf2$^-$Tomato$^-$
Ebf2$^-$Tomato$^+$
Tomato
Ebf2$^+$Tomato$^+$
Ebf2$^+$Tomato$^+$CD44$^-$
Ebf2$^+$Tomato$^-$
Ebf2$^+$Tomato$^-$CD44$^-$
Ebf2$^-$Tomato$^+$
Ebf2$^-$Tomato$^+$CD44$^-$
Ebf2$^-$Tomato$^-$
Ebf2$^-$Tomato$^-$CD44$^-$
SCA1
CD140a
CD44
Ebf2$^+$ PαS
Ebf2$^-$ PαS
E
Ebf2$^+$Tomato$^+$
Ebf2$^-$Tomato$^+$
% Ebf2$^+$Tomato$^+$ of CD45$^-$TER119$^-$CD31$^-$
% Ebf2$^-$Tomato$^+$ of CD45$^-$TER119$^-$CD31$^-$
ns
*
Months after tamoxifen injection
F
within Ebf2$^-$Tomato$^+$ cells
% CD140a$^+$SCA1$^+$ (PαS)
% CD140a$^+$SCA1$^-$
***
G
Ebf2
Tomato
CD31
DAPI

Figure 4

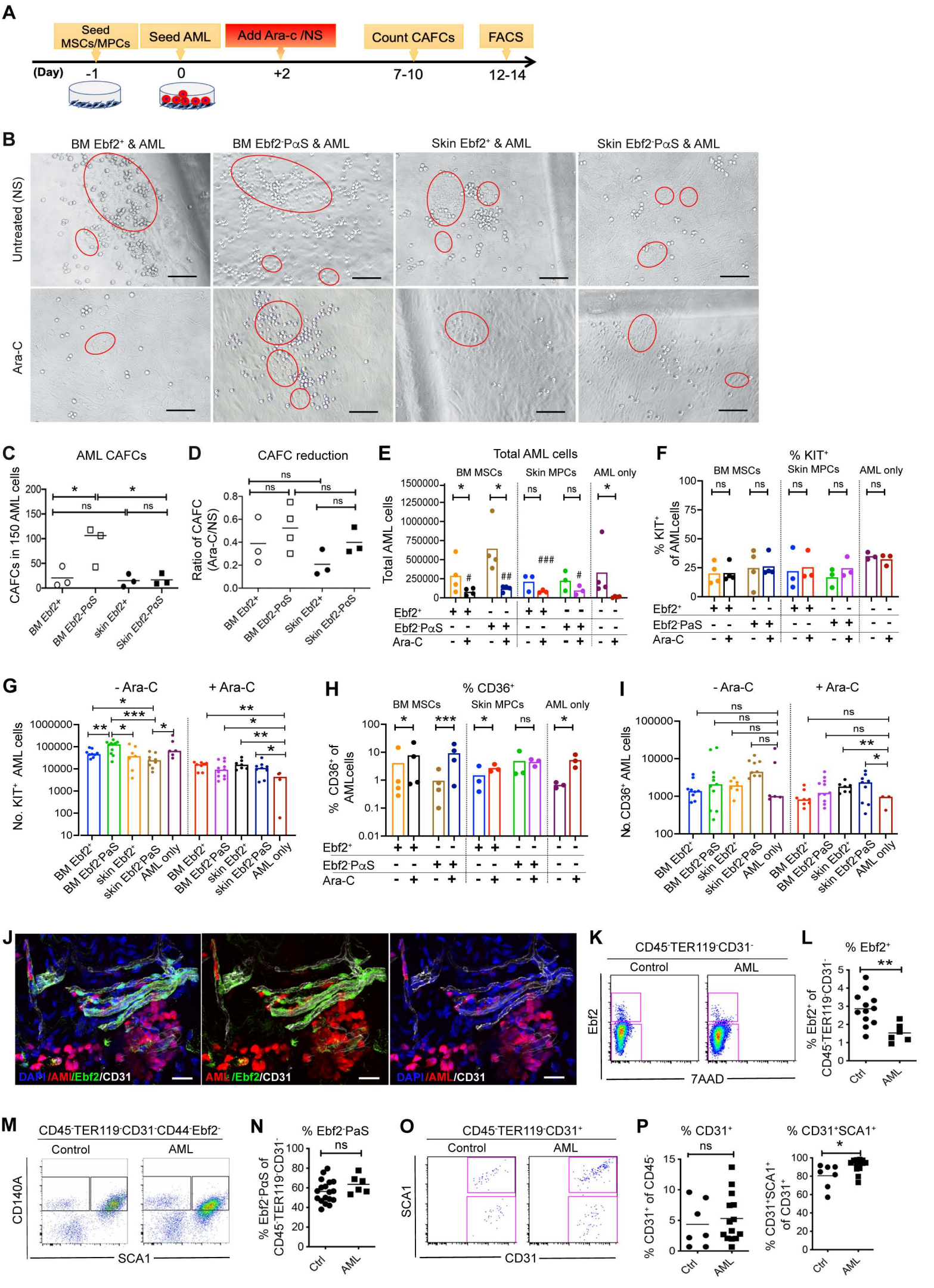
A
Seed MSCs/MPCs
Seed AML
Add Ara-c /NS
Count CAFCs
FACS
(Day)
-1
0
+2
7-10
12-14
B
BM Ebf2+ & AML
BM Ebf2-PαS & AML
Skin Ebf2+ & AML
Skin Ebf2-PαS & AML
Untreated (NS)
Ara-C
C
AML CAFCs
CAFCs in 150 AML cells
BM Ebf2+
BM Ebf2-PαS
skin Ebf2+
Skin Ebf2-PαS
D
CAFC reduction
Ratio of CAFC (Ara-C/NS)
E
Total AML cells
BM MSCs
Skin MPCs
AML only
Total AML cells
Ebf2+
Ebf2-PαS
Ara-C
F
% KIT+
% KIT+ of AMLcells
G
- Ara-C
+ Ara-C
No. KIT+ AML cells
H
% CD36+
% CD36+ of AMLcells
I
No. CD36+ AML cells
J
DAPI/AML/Ebf2/CD31
AML/Ebf2/CD31
DAPI/AML/CD31
K
CD45-TER119-CD31-
Control
AML
Ebf2
7AAD
L
% Ebf2+
% Ebf2+ of CD45-TER119-CD31-
Ctrl
AML
M
CD45-TER119-CD31-CD44-Ebf2-
CD140A
SCA1
N
% Ebf2-PaS
% Ebf2-PαS of CD45-TER119-CD31-
O
CD45-TER119-CD31+
SCA1
CD31
P
% CD31+
% CD31+ of CD45-
% CD31+SCA1+
% CD31+SCA1+ of CD31+

Figure 5

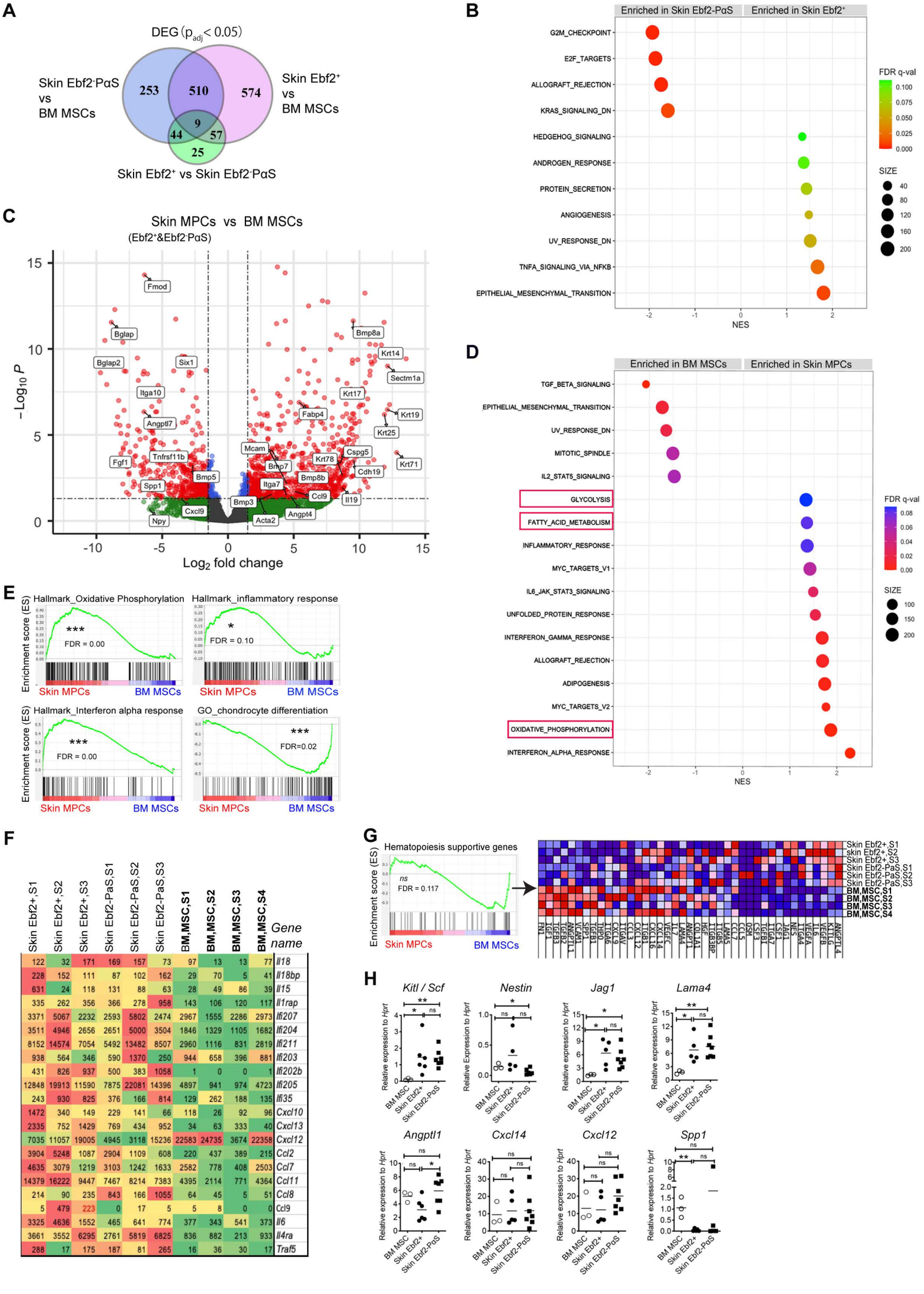
A
DEG (p_{adj} < 0.05)
Skin Ebf2⁻PαS vs BM MSCs
Skin Ebf2⁺ vs BM MSCs
Skin Ebf2⁺ vs Skin Ebf2⁻PαS
253
510
574
9
44
57
25
B
Enriched in Skin Ebf2-PαS
Enriched in Skin Ebf2⁺
G2M_CHECKPOINT
E2F_TARGETS
ALLOGRAFT_REJECTION
KRAS_SIGNALING_DN
HEDGEHOG_SIGNALING
ANDROGEN_RESPONSE
PROTEIN_SECRETION
ANGIOGENESIS
UV_RESPONSE_DN
TNFA_SIGNALING_VIA_NFKB
EPITHELIAL_MESENCHYMAL_TRANSITION
NES
FDR q-val
SIZE
C
Skin MPCs vs BM MSCs
(Ebf2⁺&Ebf2⁻PαS)
– Log10 P
Log2 fold change
Fmod
Bglap
Bglap2
Six1
Itga10
Angptl7
Fgf1
Tnfrsf11b
Spp1
Bmp5
Cxcl9
Npy
Bmp3
Acta2
Angpt4
Mcam
Bmp7
Itga7
Bmp8b
Ccl9
Il19
Cdh19
Krt78
Cspg5
Fabp4
Krt17
Bmp8a
Krt14
Sectm1a
Krt19
Krt25
Krt71
D
Enriched in BM MSCs
Enriched in Skin MPCs
TGF_BETA_SIGNALING
EPITHELIAL_MESENCHYMAL_TRANSITION
UV_RESPONSE_DN
MITOTIC_SPINDLE
IL2_STAT5_SIGNALING
GLYCOLYSIS
FATTY_ACID_METABOLISM
INFLAMMATORY_RESPONSE
MYC_TARGETS_V1
IL6_JAK_STAT3_SIGNALING
UNFOLDED_PROTEIN_RESPONSE
INTERFERON_GAMMA_RESPONSE
ALLOGRAFT_REJECTION
ADIPOGENESIS
MYC_TARGETS_V2
OXIDATIVE_PHOSPHORYLATION
INTERFERON_ALPHA_RESPONSE
NES
FDR q-val
SIZE
E
Hallmark_Oxidative Phosphorylation
FDR = 0.00
Hallmark_inflammatory response
FDR = 0.10
Hallmark_Interferon alpha response
FDR = 0.00
GO_chondrocyte differentiation
FDR=0.02
Enrichment score (ES)
Skin MPCs
BM MSCs
F
Skin Ebf2+,S1
Skin Ebf2+,S2
Skin Ebf2+,S3
Skin Ebf2-PaS,S1
Skin Ebf2-PaS,S2
Skin Ebf2-PaS,S3
BM,MSC,S1
BM,MSC,S2
BM,MSC,S3
BM,MSC,S4
Gene name
122 32 171 169 157 73 97 13 13 77 Il18
228 152 111 87 102 162 29 70 5 41 Il18bp
631 24 118 131 88 63 28 49 86 39 Il15
335 262 356 366 278 958 143 106 120 117 Il1rap
3371 5067 2232 2593 5802 2474 2967 1555 2286 2973 Ifi207
3511 4946 2656 2651 5000 3504 1846 1329 1105 1682 Ifi204
8152 14574 7054 5492 13482 8507 2960 1116 831 2819 Ifi211
938 564 346 590 1370 250 944 658 396 881 Ifi203
431 826 937 500 383 1058 1 0 0 1 Ifi202b
12848 19913 11590 7875 22081 14396 4897 941 974 4723 Ifi205
243 930 825 376 166 814 129 262 188 135 Ifi35
1472 340 149 229 141 66 118 26 92 96 Cxcl10
2335 752 1429 769 434 952 34 63 333 40 Cxcl13
7035 11057 19005 4945 3118 15236 22583 24735 3674 22358 Cxcl12
3904 5248 1087 2904 1109 608 220 437 389 215 Ccl2
4635 3079 1219 3103 1242 1633 2582 778 408 2503 Ccl7
14379 16222 9447 7467 8214 7383 4395 2114 771 4364 Ccl11
214 90 235 843 166 1055 64 45 5 51 Ccl8
5 479 223 0 17 5 5 8 0 0 Ccl9
3325 4636 1552 465 641 774 377 343 541 373 Il6
3661 3552 6295 2761 5819 6825 836 882 213 933 Il4ra
288 17 175 187 81 265 16 36 30 17 Traf5
G
Hematopoiesis supportive genes
ns
FDR = 0.117
Enrichment score (ES)
Skin MPCs
BM MSCs
Skin Ebf2+,S1
Skin Ebf2+,S2
Skin Ebf2+,S3
Skin Ebf2-PaS,S1
Skin Ebf2-PaS,S2
Skin Ebf2-PaS,S3
BM,MSC,S1
BM,MSC,S2
BM,MSC,S3
BM,MSC,S4
H
Kitl / Scf
Nestin
Jag1
Lama4
Angptl1
Cxcl14
Cxcl12
Spp1
Relative expression to Hprt
BM MSC
Skin Ebf2+
Skin Ebf2-PaS

Figure 6

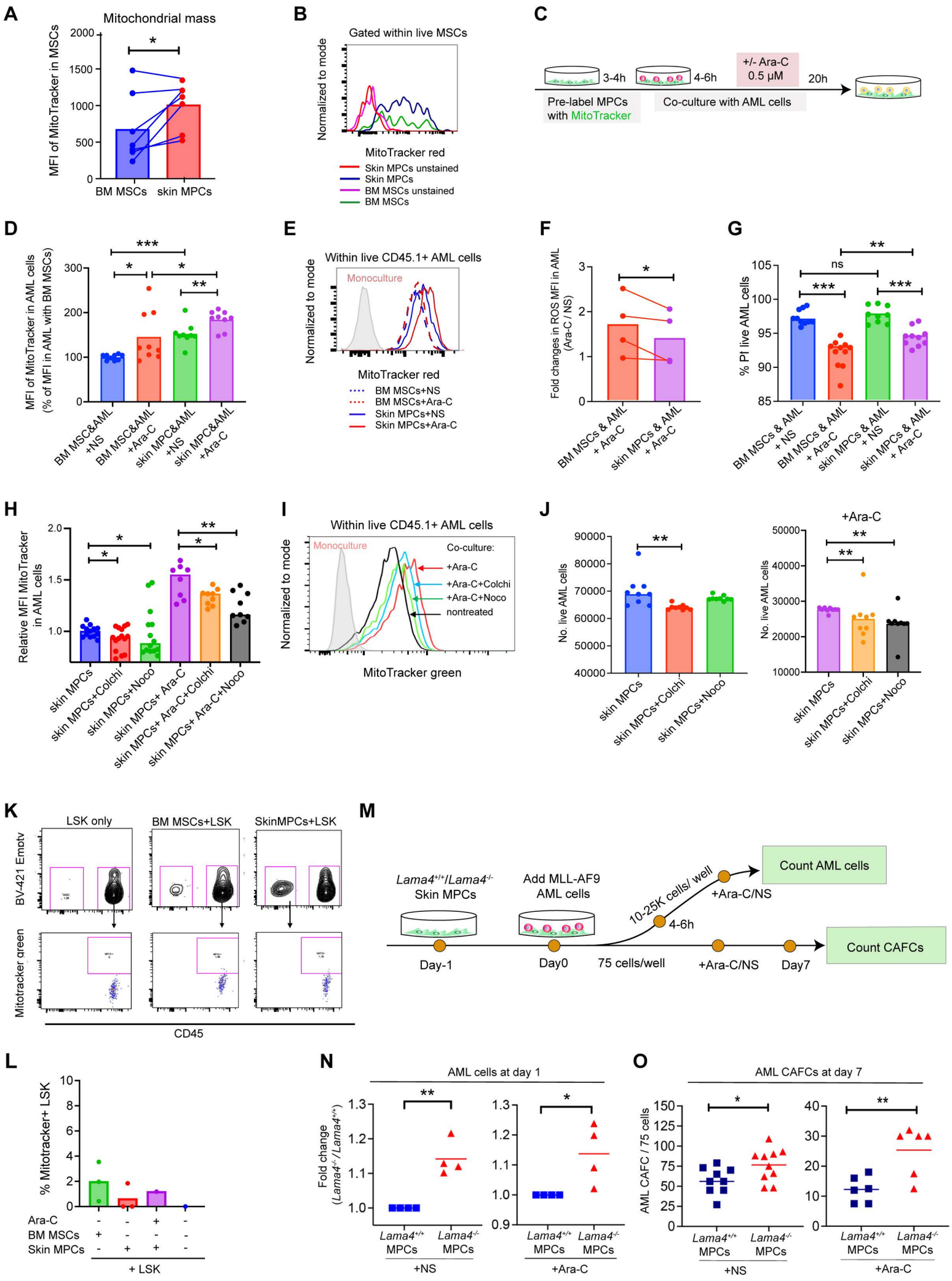
A
Mitochondrial mass
MFI of MitoTracker in MSCs
BM MSCs
skin MPCs
B
Gated within live MSCs
Normalized to mode
MitoTracker red
Skin MPCs unstained
Skin MPCs
BM MSCs unstained
BM MSCs
C
3-4h
4-6h
+/- Ara-C
0.5 μM
20h
Pre-label MPCs
with MitoTracker
Co-culture with AML cells
D
MFI of MitoTracker in AML cells
(% of MFI in AML with BM MSCs)
BM MSC&AML +NS
BM MSC&AML +Ara-C
skin MPC&AML +NS
skin MPC&AML +Ara-C
E
Within live CD45.1+ AML cells
Monoculture
Normalized to mode
MitoTracker red
BM MSCs+NS
BM MSCs+Ara-C
Skin MPCs+NS
Skin MPCs+Ara-C
F
Fold changes in ROS MFI in AML
(Ara-C / NS)
BM MSCs & AML + Ara-C
skin MPCs & AML + Ara-C
G
% PI live AML cells
ns
BM MSCs & AML + NS
BM MSCs & AML + Ara-C
skin MPCs & AML + NS
skin MPCs & AML + Ara-C
H
Relative MFI MitoTracker in AML cells
skin MPCs
skin MPCs+Colchi
skin MPCs+Noco
skin MPCs+ Ara-C
skin MPCs+ Ara-C+Colchi
skin MPCs+ Ara-C+Noco
I
Within live CD45.1+ AML cells
Monoculture
Co-culture:
+Ara-C
+Ara-C+Colchi
+Ara-C+Noco
nontreated
Normalized to mode
MitoTracker green
J
No. live AML cells
skin MPCs
skin MPCs+Colchi
skin MPCs+Noco
+Ara-C
K
LSK only
BM MSCs+LSK
SkinMPCs+LSK
BV-421 Empty
Mitotracker green
CD45
M
Lama4+/+/Lama4-/-
Skin MPCs
Add MLL-AF9
AML cells
10-25K cells/ well
+Ara-C/NS
Count AML cells
4-6h
Day-1
Day0
75 cells/well
+Ara-C/NS
Day7
Count CAFCs
L
% Mitotracker+ LSK
Ara-C
BM MSCs
Skin MPCs
+ LSK
N
AML cells at day 1
Fold change
(Lama4-/-/Lama4+/+)
Lama4+/+ MPCs
Lama4-/- MPCs
+NS
+Ara-C
O
AML CAFCs at day 7
AML CAFC / 75 cells
Lama4+/+ MPCs
Lama4-/- MPCs
+NS
+Ara-C

Figure 7

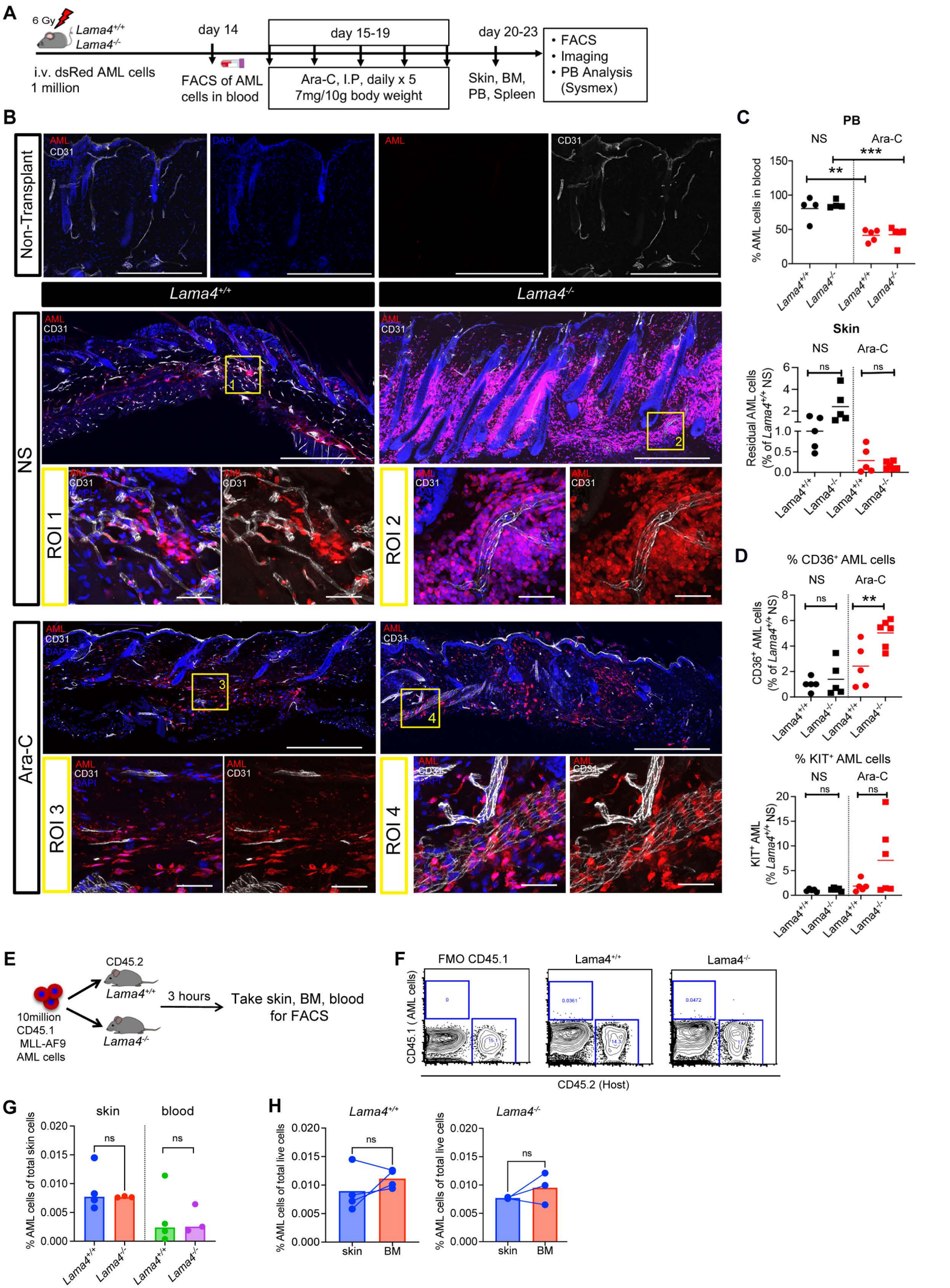
A
6 Gy
Lama4+/+
Lama4-/-
i.v. dsRed AML cells
1 million
day 14
FACS of AML cells in blood
day 15-19
Ara-C, I.P, daily x 5
7mg/10g body weight
day 20-23
Skin, BM, PB, Spleen
• FACS
• Imaging
• PB Analysis (Sysmex)
B
Non-Transplant
AML
CD31
DAPI
Lama4+/+
Lama4-/-
NS
ROI 1
ROI 2
Ara-C
ROI 3
ROI 4
C
PB
NS
Ara-C
% AML cells in blood
Skin
Residual AML cells (% of Lama4+/+ NS)
D
% CD36+ AML cells
CD36+ AML cells (% of Lama4+/+ NS)
% KIT+ AML cells
KIT+ AML (% Lama4+/+ NS)
E
CD45.2
Lama4+/+
Lama4-/-
10million
CD45.1
MLL-AF9
AML cells
3 hours
Take skin, BM, blood for FACS
F
FMO CD45.1
CD45.1 (AML cells)
CD45.2 (Host)
G
skin
blood
% AML cells of total skin cells
H
% AML cells of total live cells
skin
BM

Figure 8

A

Experimental setup for assessing residual AML-initiating LSCs in the skin

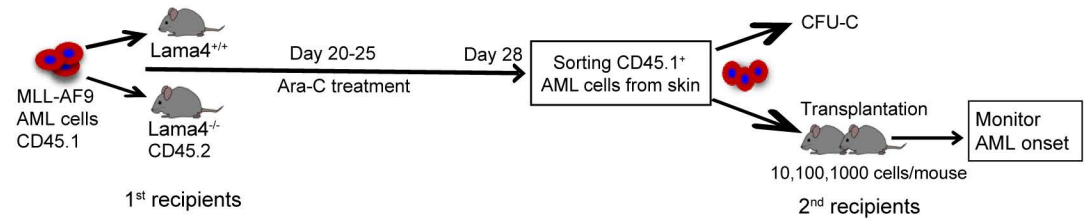

B

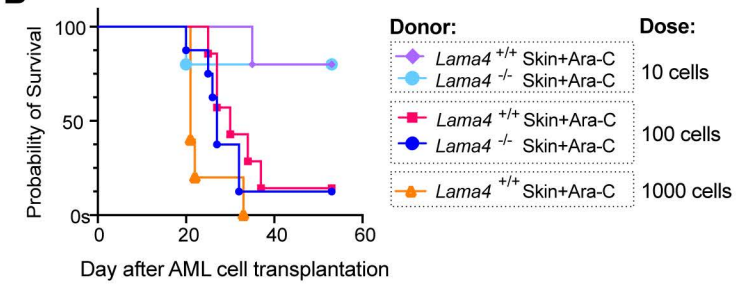

C

Frequency of AML-initiating LSCs in AML cells from skin post-Ara-C

Donor mice	Cell Origin	# mice: AML mice /total 2nd recipients				Frequency of AML Initiating LSCs	
		cell dose: 5000	1000	100	10		
Lama4 $^{+/+}$	Skin	2/2	5/5	6/7	1/5	1/51	ns
Lama4 $^{-/-}$	Skin	N/A	N/A	7/8	1/5	1/48	

D

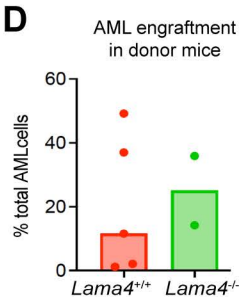
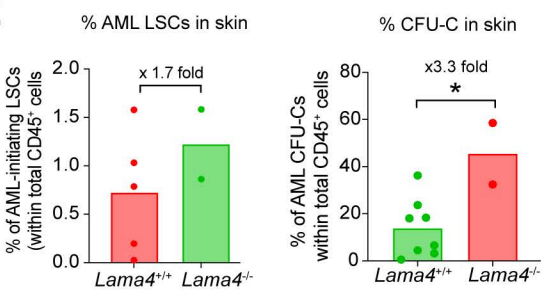
E